atmosphere

MDPI

Article

The Proportional Characteristics of Daytime and Nighttime Precipitation Based on Daily Precipitation in Huai River Basin, China

Ying Zhu [1], Xiaoli Liu [1,*], Yuqing Zhang [2], Changchun Chen [3], Liucheng Shen [4], Qin Ju [5], Ting Zhou [1] and Ping Xia [1]

[1] School of Engineering, Anhui Agricultural University, Hefei 230036, China
[2] School of Urban and Environmental Sciences, Huaiyin Normal University, Huai'an 223300, China
[3] School of Geographical Sciences, Nanjing University of Information Science & Technology, Nanjing 210044, China
[4] School of Environmental and Geographical Sciences, Shanghai Normal University, Shanghai 200234, China
[5] State Key Laboratory of Hydrology-Water Resources and Hydraulic Engineering, Hohai University, Nanjing 210098, China
* Correspondence: xiaoli_liu@ahau.edu.cn

Abstract: The daytime and nighttime precipitation proportions of daily total precipitation (especially extreme daily precipitation) are important indicators that help to understand the process of precipitation formation, which in turn helps to evaluate and improve models and reanalysis precipitation data. In this study, we used the Huai River Basin (HRB) as a case to explore the daytime and nighttime precipitation proportions of daily total precipitation based on 135 meteorological stations during 1961–2018. The total, daytime, and nighttime precipitation showed zonal distributions with high and low values in the southern and northern parts of the basin, respectively. The nighttime precipitation was slightly greater than the daytime precipitation. With the increase in precipitation intensity, the seasonal cycles of the total, daytime, and nighttime precipitation were more distinct, and precipitation mainly occurred in summer. The annual range of precipitation differences between daytime and nighttime in wet seasons showed a downward trend in 1961–2003 followed by an upward trend in 2003–2018. This reversal of annual range of precipitation around 2003 may be related to the changes in annual range of convective precipitation differences between daytime and nighttime in wet seasons. The decrease of light precipitation mainly depended on the decrease of nighttime precipitation. The contributions of nighttime precipitation events to torrential precipitation events were greater than those of daytime precipitation. The days of extreme precipitation events accounted for a very low proportion of total precipitation days, but their precipitation amount accounted for relatively high proportions of total precipitation amount. Annual extreme precipitation amount showed a slightly upward trend, which was caused by the increased nighttime precipitation. Under extreme precipitation conditions, large proportions of daytime precipitation were mainly concentrated in the southeastern parts of the HRB, whereas large proportions of nighttime precipitation were mainly concentrated in the northwestern parts of the basin. The concurrent daytime and nighttime precipitation showed slightly increasing trends, especially in the southeastern part of the basin. With the increase in daytime and nighttime precipitation, the risk of concurrent precipitation extremes in the southern part of the basin increased (shorter return period means higher risk).

Keywords: daytime and nighttime precipitation; precipitation extremes; copula; Huai River Basin

Citation: Zhu, Y.; Liu, X.; Zhang, Y.; Chen, C.; Shen, L.; Ju, Q.; Zhou, T.; Xia, P. The Proportional Characteristics of Daytime and Nighttime Precipitation Based on Daily Precipitation in Huai River Basin, China. *Atmosphere* **2022**, *13*, 1287. https://doi.org/10.3390/atmos13081287

Academic Editor: Anita Drumond

Received: 30 June 2022
Accepted: 11 August 2022
Published: 13 August 2022

1. Introduction

Currently, the global temperature rises at a high rate, but the linear trend of long-term precipitation may be weak and generally shows obvious fluctuation characteristics [1,2]. The diurnal variation of precipitation is accompanied by the thermal and dynamic daily cycle processes of water and energy fluxes [3–5], which may affect the long-term precipitation fluctuations. The exploration of the diurnal cycle characteristics of precipitation not only

helps to understand physical processes of precipitation, but it also allows the optimization of weather/climate models to improve the accuracy of precipitation forecasts [6–9]. Generally, precipitation peaks mainly exist in the afternoon and nighttime. The afternoon convective precipitation is usually caused by the instability of the low-level atmosphere and water vapor convergence due to solar heating [3,10,11]. Nocturnal precipitation is usually due to radiative cooling at night, which causes the condensation of substantial amount of water vapor [3,4,12]. There are different characteristics and mechanisms of diurnal precipitation cycles in different regions. For instance, the nighttime precipitation peaks in the middle and lower reaches of the Yangtze River may be caused by the Meiyu front, or they may be related to the propagation of the precipitation systems caused by the mid-latitude westerly flow [13–15]. The precipitation peaks in the Sichuan basin and the eastern margin of the Tibetan Plateau during nighttime are mainly affected by topographical features [4,12,16].

The diurnal variation of precipitation may be affected by the duration of multiple intermittent precipitation events in a day [4,17]. In accordance with their lengths, precipitation events can be divided into short ($\leq$3 h) and long ($\geq$6 h) durations. The former are usually caused by local convective precipitation (usually occurs in the afternoon), and the latter are usually related to large-scale precipitation (usually occurs in the evening to early morning) [10,13,14,17]. Large-scale precipitation refers to the steady, sustained rain or snow associated with large-scale forced ascent or detrainment, and convective precipitation refers to the intermittent burst of liquid or solid precipitation, associated with local convective air circulation [18]. Precipitation that lasts for several hours may be potentially destructive, such as flash floods [19]. Therefore, the characteristics of precipitation on the sub-daily timescale (daytime and nighttime) are receiving attention. The previous studies [3,7,20] on the seasonal, annual, and even extreme daytime and nighttime precipitation were generally determined using individual daytime or nighttime precipitation, which may ignore the complete day event scale.

The enhancement of the annual precipitation difference (range) between wet and dry seasons may intensify extreme conditions (more floods or droughts) [21]. Therefore, it is necessary to investigate characteristics of the differences between daytime and nighttime precipitation during wet and dry seasons. Analyzing the characteristics of daytime and nighttime precipitation at different intensity levels aids in developing an in-depth understanding of the diurnal precipitation cycle. Previous studies mainly explored the characteristics of different intensities of precipitation using hourly or sub-daily precipitation data [3,7,19,22]. However, it is also important to use indicators of complete daily precipitation intensity to explore the proportional characteristics of the daytime and nighttime precipitation. The proportions of daytime and nighttime precipitation under different daily total precipitation intensities aid in our understanding of the precipitation diurnal cycle and related mechanisms.

Precipitation extremes have significant impacts on the ecosystems, socio-economies, and human health, as illustrated by the storm events that occurred on 20 July 2021 in Henan and 20 July 2016 in Beijing, China [23–25]. There have been some studies on hourly extreme precipitation [19,26], but the proportions of daytime and nighttime precipitation during extreme precipitation events using complete-day data have not yet been explored. The destructive power of extreme precipitation events caused by consecutive precipitation (several days) is generally greater than that of a single hour or daily extreme precipitation. For example, the 2020 super long Meiyu season in the Yangtze and Huai River basins in China [27], and the heavy precipitation in the Sichuan Basin in China during 10–18 August 2020 [28]. The investigation of daytime and nighttime precipitation proportions during consecutive extreme precipitation events may be helpful to increase our understanding of the consecutive extreme precipitation processes and further improve extreme precipitation predictions.

The return level and return period of extreme precipitation provide critical information for decision-making and risk assessment [29,30]. Typically, risk assessments are based on

one natural indicator under a univariate framework, such as extreme heat based on high percentile thresholds for the maximum temperature [31]. The univariate estimates of return periods may be less accurate in assessing concurrent events, leading to underestimations of the risks of extreme conditions [32]. The combination of different proportions of daytime and nighttime precipitation with the same total daily extreme precipitation may lead to different risk degrees of extreme precipitation events, which is a signal that cannot be detected by the total daily precipitation. In fact, traditional risk assessment based on daily extreme precipitation may not accurately represent concurrent daytime and nighttime precipitation extremes and could lead to the underestimation of the risks of precipitation extremes. Therefore, it is necessary to evaluate the risks of concurrent precipitation extremes under different combinations of daytime and nighttime precipitation based on multidimensional joint distribution function method.

We used the Huai River Basin (HRB) as a case study to investigate the proportional characteristics of daytime and nighttime precipitation from daily precipitation. The objectives of this study were as follows: (1) explore the spatio-temporal characteristics of annual daytime and nighttime precipitation; (2) investigate annual range of precipitation difference between daytime and nighttime in wet/dry seasons; (3) elucidate the daytime and nighttime precipitation proportions at different intensity levels of daily precipitation events; (4) determine the daytime and nighttime precipitation proportions using daily extreme precipitation indices; and (5) characterize risks of concurrent daytime and nighttime precipitation extremes using a multivariate copula method. The findings presented here may enrich our knowledge of the diurnal cycles of precipitation and provide valuable insights into the ecological and social consequences caused by daytime and nighttime precipitation extremes that can be used by decision-makers responsible for determining mitigation strategies.

2. Materials and Methods

2.1. Study Area

The HRB lies between the middle and lower reaches of the Yangtze River and the middle and lower reaches of the Yellow River. The HRB covers an approximate area of 270,000 km^2 in the eastern parts of China (approximately 112–121° E, 31–36° N) and belongs to a climate transitional zone between the humid and semi-humid monsoon regions (Figure 1). The elevation of most parts of HRB is less than 100 m above sea level (a.s.l), especially the vast plain in the eastern parts of the basin. Since the HRB is dominated by plains, precipitation and temperature mainly show zonal distribution characteristics. Annual mean precipitation decreases from about 1200 mm in the southern parts of the basin to about 700 mm in the northern parts of the basin [33]. The annual mean temperature ranges from about 11 °C in the northern parts of the basin to about 16 °C in the southern parts of the basin [34]. In the summer, the HRB is controlled by the Meiyu front and subtropical high systems that make it prone to flood and drought events [35]. The HRB is an important commodity grain base in China due to the characteristics of climate and topography [36]. The contributions of daytime and nighttime precipitation to extreme precipitation play important roles in the growth of crops in the HRB.

2.2. Data

Daytime (08:00−20:00 BT), nighttime (20:00−08:00 BT), and total (daily, 20:00−20:00 BT) precipitation for 1961−2018 were derived from the China Meteorological Administration (http://data.cma.cn/ (accessed on 1 June 2022)). The dataset underwent quality control and homogeneity testing before its release. The station was excluded if its daytime, nighttime, or total precipitation data were missing for more than 31 days (≥0.15% missing data) during 1961−2018. Missing values (<0.15% missing data) for the station was interpolated using the average value of 10 neighboring stations on the same timestep. Finally, 135 meteorological stations (Figure 1) spanning 1961−2018 across the HRB were selected for this study.

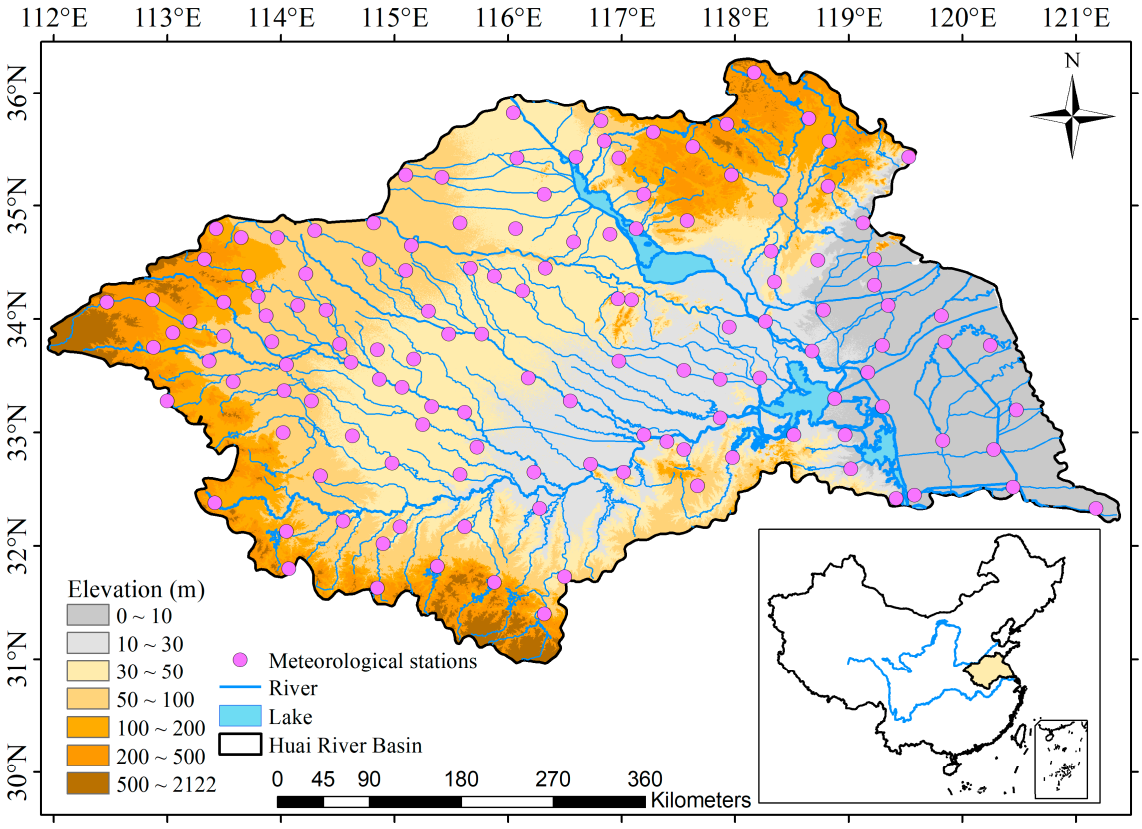

Figure 1. Location of Huai River Basin and its 135 meteorological stations.

ERA5 is the new fifth-generation reanalysis dataset released by the European Centre for Medium Range Weather Forecasts (ECMWF) [37] that contains a large number of hydrometeorological variables with high spatiotemporal resolution. It has been widely applied in hydrometeorological investigations and evaluations worldwide [1,38–40]. The ERA5 variables including total, large-scale, and convective precipitation (a spatial resolution of 0.25° and hourly temporal resolution) from 1961 to 2018 were used in this study. We integrated the ERA5 dataset into daytime (08:00−20:00 BT) and nighttime (20:00−08:00 BT) sequences. We extracted the ERA5 grid nearest to the location of the observed station (i.e., grid point closest to the station) for data comparisons and analyses.

2.3. Definitions of Wet and Dry Seasons

We defined the dry and wet seasons as follows [21]: we first calculated the 3-month running averages (precipitation) for each station from 1961 to 2018, and then we defined the maximum value of the 3-month running average value in each year as the wet season and the minimum value as the dry season. Thus, the wet and dry seasons vary with the year and location (station). We calculated the difference between daytime and nighttime precipitation during the wet/dry seasons to obtain annual range of precipitation.

2.4. Different Grades of Precipitation Intensity

A precipitation event is generally defined as a precipitation amount (p) of no less than 0.1 mm/day [41–43]. The China Meteorological Administration generally provided four grades of daily precipitation intensity (http://www.cma.gov.cn/2011xzt/2012zhuant/20120928_1_1_1_1/2010052703/201212/t20121212_195616.html (accessed on 1 June 2022)) as follows: light ($0.1 \leq p < 10$ mm/day), moderate ($10 \leq p < 25$ mm/day), heavy ($25 \leq p < 50$ mm/day), and torrential ($\geq$50 mm/day). This study applied the total daily timescale to define the grades of precipitation intensity and then explored the characteristics of daytime and nighttime precipi-

tation at different grades. Thus, we were able to investigate the distribution characteristics of daytime and nighttime precipitation when the total daily precipitation reaches a certain grade.

2.5. Precipitation Extremes

Annual maximum consecutive 5-day precipitation amount (RX5day) is an important extreme precipitation index, and a large RX5day value can induce a flood disaster. Let RR_{kj} be the precipitation amount for the 5-day interval ending k, period j. The maximum consecutive 5-day values for period j are:

$$RX5day = max\left(RR_{kj}\right) \tag{1}$$

This study used the daily total precipitation to calculate the RX5day at each station from 1961 to 2018, and then we investigated the daytime and nighttime proportions. Let RR_{wj} be the daily precipitation amount on a wet day w ($\geq$0.1 mm) in period j and let $RR90$ be the 90th percentile of precipitation on wet days in the 1961−2018 period. If n represents the number of wet days in the period, then:

$$TR90p = \sum_{w=1}^{n} RR_{wj} \; where \; RR_{wj} > RR90 \tag{2}$$

TR90p represents the annual total precipitation when total daily precipitation >90th percentile of the local all wet days during 1961−2018. We separately explored the daytime and nighttime precipitation proportions under TR90p conditions. DR90p and NR90p represent daytime and nighttime precipitation greater than 90th percentiles of the local daytime and nighttime wet days during 1961−2018, respectively (similar to Equation (2)). Concurrent extreme daytime and nighttime precipitation (CEDNP) was defined in this study as simultaneously meeting the conditions (the same day) of daytime and nighttime precipitation greater than the 90th percentiles of their respective local daytime and nighttime wet days during 1961−2018. We investigated the proportions of daytime and nighttime precipitation under CEDNP conditions.

2.6. Copula Method

Copulas are joint distribution functions that can construct the dependence structure of two or more time-independent variables regardless of their original marginal distributions [44–47]. We applied the copula method to explore return periods of the CEDNP based on the different combinations of daytime and nighttime precipitation in the HRB. The marginal distributions of daytime (X) and nighttime (Y) precipitation under CEDNP events were first established. We used some continuous marginal distribution functions to select a suitable model that optimally fit the variables X and Y. These marginal distribution functions included: Beta, Birnbaum–Saunders, Exponential, Extreme value, Gamma, Generalized extreme value, Generalized Pareto, Inverse Gaussian, Logistic, Log-logistic, Lognormal, Nakagami, Normal, Rayleigh, Rician, t location-scale, and Weibull distributions [46]. The optimal marginal function was selected via the Bayesian Information Criterion (BIC), and the parameters of the marginal distributions were calculated via the Maximum Likelihood Method (MLE) to minimize the distances between their model and empirical probabilities [45,46,48].

Assuming two variables X and Y with cumulative distribution functions F_X and F_Y, respectively, a two-dimensional copula (C) can establish their joint distribution as follows:

$$F(x, y) = C(F_X(x),\ F_Y(y)) = C(u, v) \tag{3}$$

where $F_X(x)$ and $F_Y(y)$ denote the cumulative distribution functions for the daytime and nighttime precipitation under CEDNP events. This study applied four commonly-used copula functions (Gaussian, Clayton, Frank, and Gumbel) in the field of hydrometeorology [47,49,50] to analyze the joint probability distributions of daytime and nighttime

precipitation under CEDNP events. The optimal copulas were selected based on the BIC, Akaike information criterion (AIC), and MLE [45,46].

If both the variables of a CEDNP simultaneously exceed the given threshold ($X \geq x$ and $Y \geq y$), then this CEDNP forms the "and (∩)" joint occurrence probability [49,51]. We applied the "and (∩)" joint return period approach to investigate the risks of CEDNP events with daytime (X) and nighttime (Y) precipitation amount exceeding the given thresholds (x and y, respectively). The joint return period was calculated as follows:

$$T(X \geq x \cap\ Y \geq y) = \frac{EL}{1 - F_X(x) - F_Y(y) + C(F_X(x),\ F_Y(y))} \quad (4)$$

where $T(X \geq x \cap\ Y \geq y)$ represents the return period (years). EL represents the average inter-arrival time of CEDNP events.

3. Results

3.1. Spatiotemporal Characteristics of Annual and Seasonal Precipitation

In the observed data, the basin-averaged annual means (1961−2018) of the total, daytime, and nighttime precipitation were 858.44, 417.69, and 440.75 mm, respectively (Figure 2). The ERA5 simulated precipitation was relatively high, especially during the daytime. The simulation effect of ERA5 precipitation under the condition of observed wet days (≥0.1 mm/day, ERA5CON) was better than that of ERA5, with correlation coefficients (r) as high as 0.88, 0.84, and 0.90 on the total, daytime, and nighttime scales, respectively. ERA5CON can reasonably reflect the characteristic that nighttime precipitation is slightly more than daytime precipitation. Total precipitation showed a slight upward trend (2.84 mm/decade), mainly due to the contribution of nighttime precipitation (3.26 mm/decade). ERA5 and ERA5CON were insufficient in simulating the long-term precipitation trend. In general, ERA5CON can reflect precipitation fluctuation characteristics and average state characteristics more reasonably than ERA5.

Exploring the long-term changing behavior of total precipitation in relation to large-scale and convective precipitation is helpful to understand the mechanism of precipitation variation. As shown in Figure 3, large-scale precipitation was approximately 15%, 18%, and 13% more than convective precipitation on the total, daytime, and nighttime scales, respectively. The annual variations in large-scale and convective precipitation were relatively consistent, but the amplitudes of large-scale precipitation were relatively large. On the total daily scale, the decline rate of convective precipitation was greater than that of large-scale precipitation, and this may be caused by the relatively large decreasing trends of convective precipitation during daytime (−6.73 mm/decade) and nighttime (−5.14 mm/decade).

The climatological pattern of total precipitation presented a zonal distribution, with more (>1100 mm) in the southern parts of the basin and less (<700 mm) in the northern parts of the basin (Figure 4a). The distribution of total precipitation days was similar to the precipitation amount, with high values (>120 days) in the southern parts of the basin and low values (<80 days) in the northern parts of the basin (Figure 4b). The multiyear averages of daytime precipitation amount (Figure 4c) and days (Figure 4d) were similar to those of the total precipitation, with a north–south gradient. The spatial characteristics of nighttime precipitation (Figure 4e,f) were also similar to those of total precipitation.

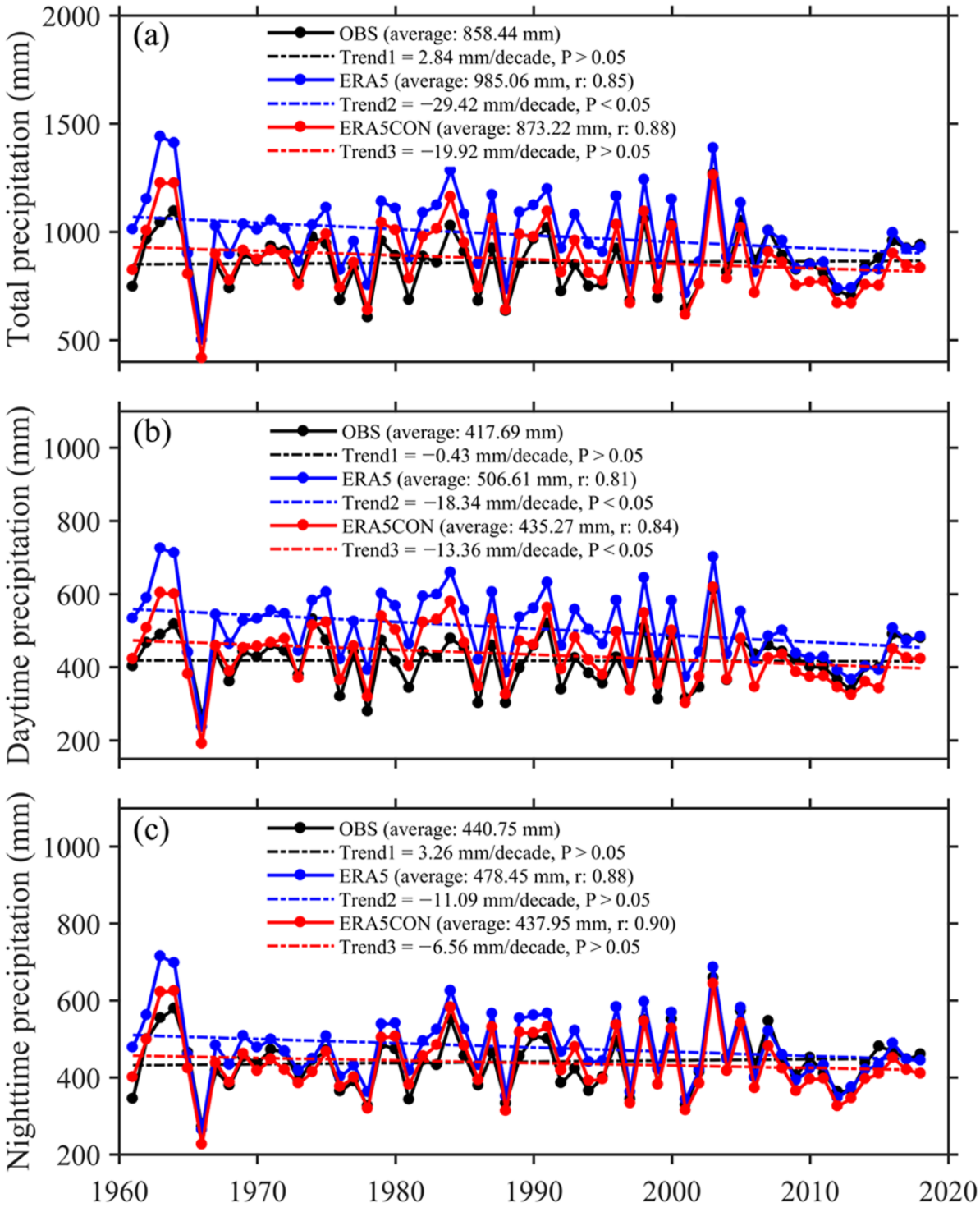

Figure 2. Annual precipitation of (**a**) total (daily), (**b**) daytime, and (**c**) nighttime precipitation per year averaged over the HRB from 1961 to 2018 in the observed, ERA5, and ERA5 under the condition of observed wet days (≥0.1 mm/day, ERA5CON), respectively. The r denotes the correlation coefficient with the observed value.

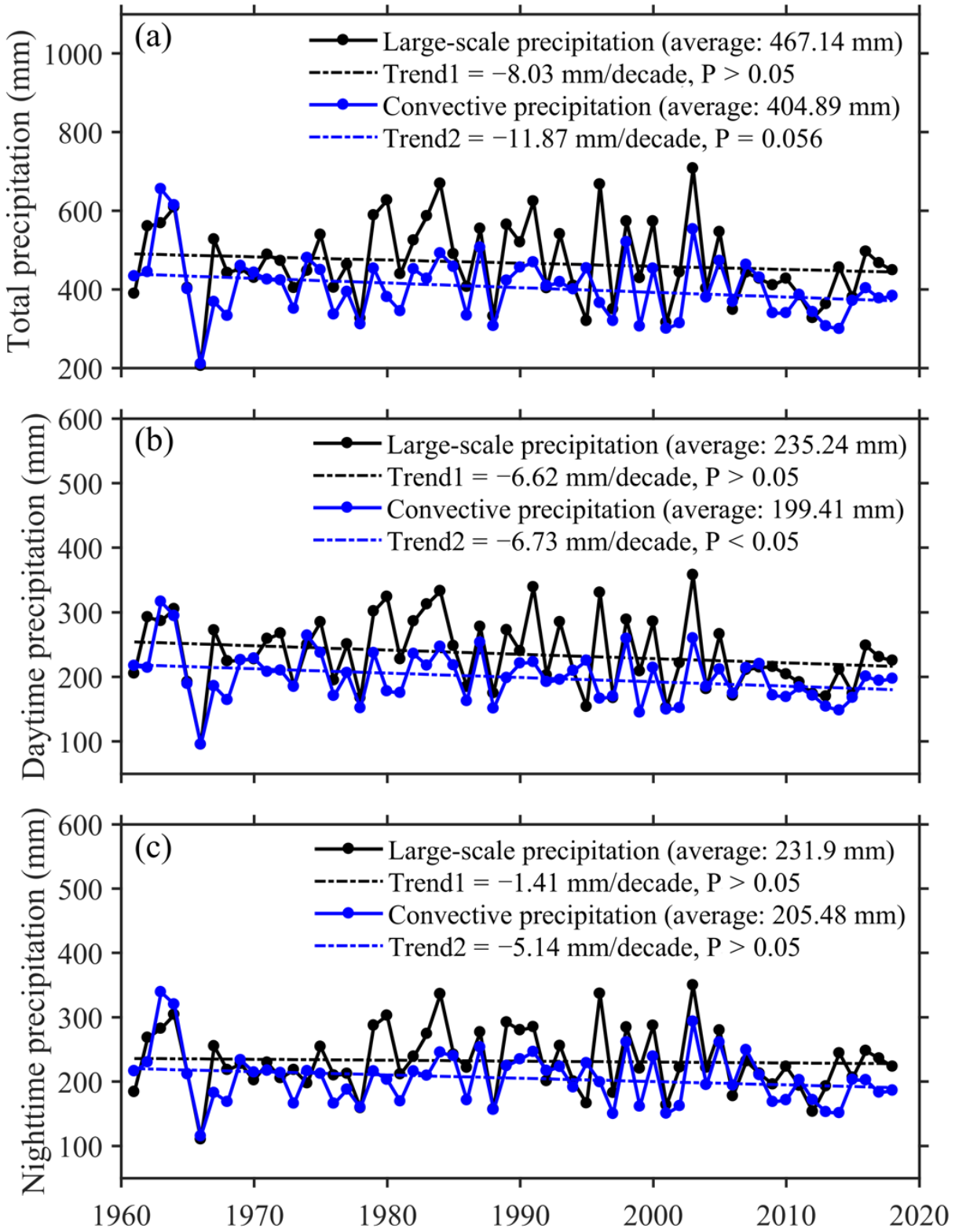

Figure 3. Annual large-scale and convective precipitation of (**a**) total (daily), (**b**) daytime, and (**c**) nighttime precipitation per year averaged over the HRB from 1961 to 2018 in the ERA5CON.

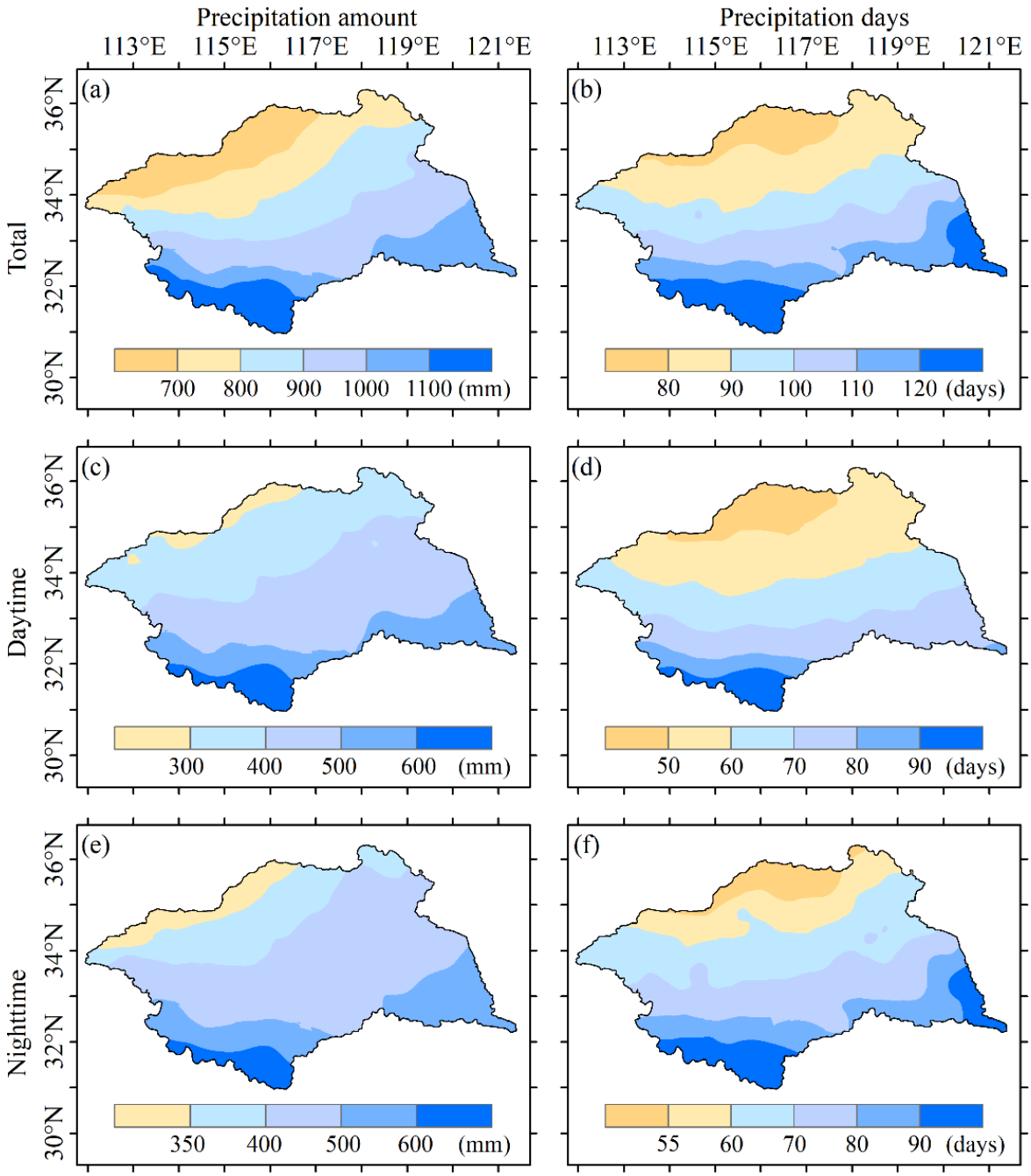

Figure 4. Spatial amount and days of (**a**,**b**) total daily, (**c**,**d**) daytime, and (**e**,**f**) nighttime precipitation in the HRB from 1961 to 2018.

As shown in Figure 5, the seasonal cycle characteristics of total, daytime, and nighttime precipitation were basically similar. The precipitation in the first half of the year showed an increasing trend, and it showed a decreasing trend after reaching its peak in July. Generally, a month with more precipitation has a larger standard deviation of precipitation (the mean increase with the standard deviation) [5]. The large standard deviation of precipitation in summer (June−August) indicates that the wide variability of precipitation may cause flood and drought events [33]. The seasonal characteristics of precipitation days were similar to the precipitation amount, but their curve shapes were flatter than those of precipitation amount (i.e., the kurtosis coefficient was relatively small), and the standard deviation appeared larger in the months with fewer precipitation days.

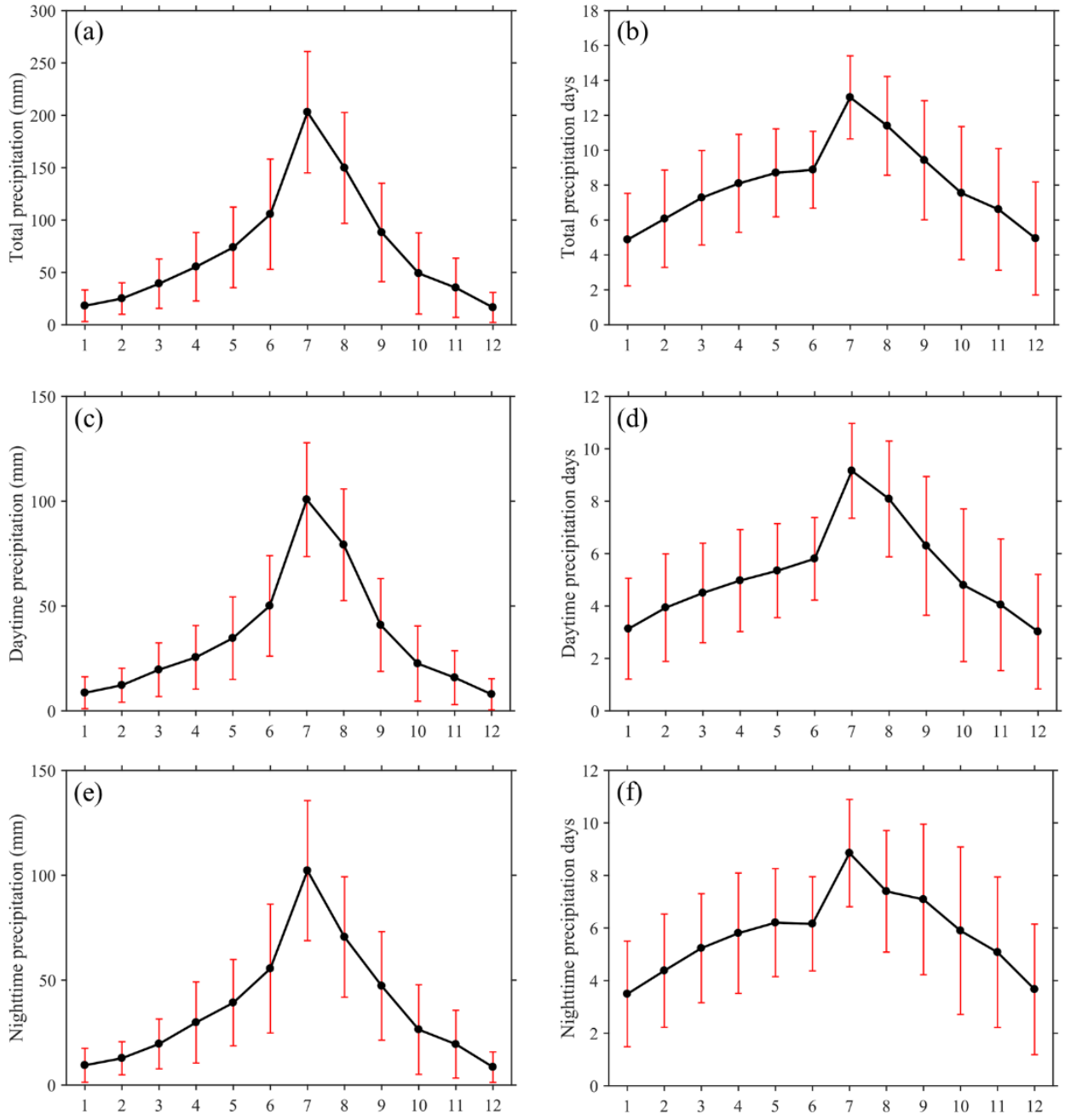

Figure 5. Climatology of monthly mean (**a**,**b**) total daily, (**c**,**d**) daytime, and (**e**,**f**) nighttime precipitation amount and days over the HRB from 1961 to 2018. Error bars (red line) represent ±1 standard deviation of the mean precipitation in each month.

As shown in Figure 6a, the nighttime precipitation was 2.14 mm/month greater than the daytime precipitation during wet seasons. We applied a piecewise linear regression method [52] to quantify potential turning points in the annual range series of precipitation during wet/dry seasons. The annual range of precipitation difference between daytime and nighttime during the wet season from 1961 to 2003 showed a significant downward trend and then a reversal (upward) trend from 2003 to 2018. The recent increasing rate of 12.52 mm/month/decade was approximately threefold greater than the decreasing rate before the turning point in 2003. The correlation coefficient between the annual daytime-nighttime precipitation range in the wet season and its large-scale precipitation was 0.25 (Figure 6b), and the correlation coefficient with the annual range of daytime-

nighttime convective precipitation reached as high as 0.64 (Figure 6c), indicating that the changes of daytime-nighttime precipitation are mainly controlled by the range of convective precipitation in wet seasons. The annual ranges of precipitation difference between daytime and nighttime in the dry seasons did not show any obvious trend characteristic (Figure 6d), and they were slightly more affected by the large-scale precipitation (r = 0.83, Figure 6e) than convective precipitation (r = 0.65, Figure 6f).

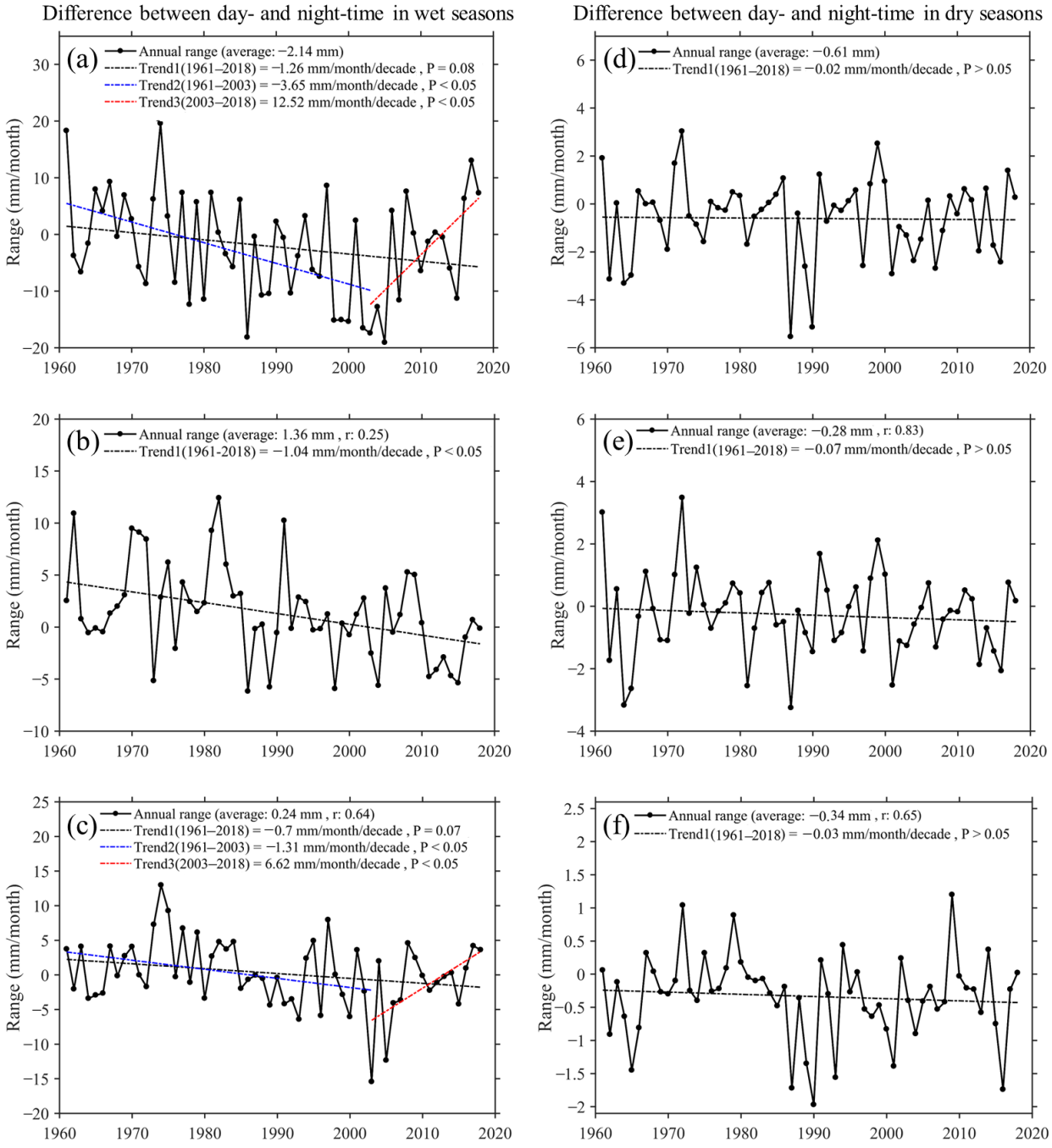

Figure 6. (**a**) Annual ranges of precipitation differences between daytime and nighttime during the wet seasons, (**b**) Annual ranges of large-scale precipitation (ERA5CON) differences between daytime and nighttime under wet season conditions using observed precipitation. (**c**) Annual ranges of convective precipitation (ERA5CON) differences between daytime and nighttime under wet season conditions using observed precipitation. (**d**−**f**) The same as (**a**–**c**), but for the dry seasons. The r denotes the correlation coefficient with the observed value (annual range).

3.2. Characteristics of Precipitation at Different Grades

As shown in Figure 7a, the average amount and days of light precipitation were 178.9 mm and 73 days, respectively. Both the light precipitation amount and days showed decreasing trends from 1961 to 2018. The average daytime precipitation (Figure 7b) at the light grade was 87.3 mm, which was slightly less than the nighttime precipitation (Figure 7c), but the decreasing trend of the daytime precipitation days (−0.8 days/decade) was obviously less than that of the nighttime precipitation days (−3.3 days/decade). The intensity of the light precipitation weakened more obviously during the nighttime than during the daytime owing to the significant increase in the difference between daytime and nighttime precipitation days (Figure 7d). Although the annual moderate precipitation was 53.3 mm more than the light precipitation, the number of moderate precipitation days was obviously less than the number of light precipitation days (Figure 7e). The moderate precipitation amount and days both showed slight upward trends, which were caused by the slight upward trends of the amount and days in both daytime (Figure 7f) and nighttime (Figure 7g) precipitation. In contrast with light precipitation events, the precipitation amount and days during daytime at the moderate grade were slightly more than those during the nighttime, and their differences showed slight upward trends (Figure 7h).

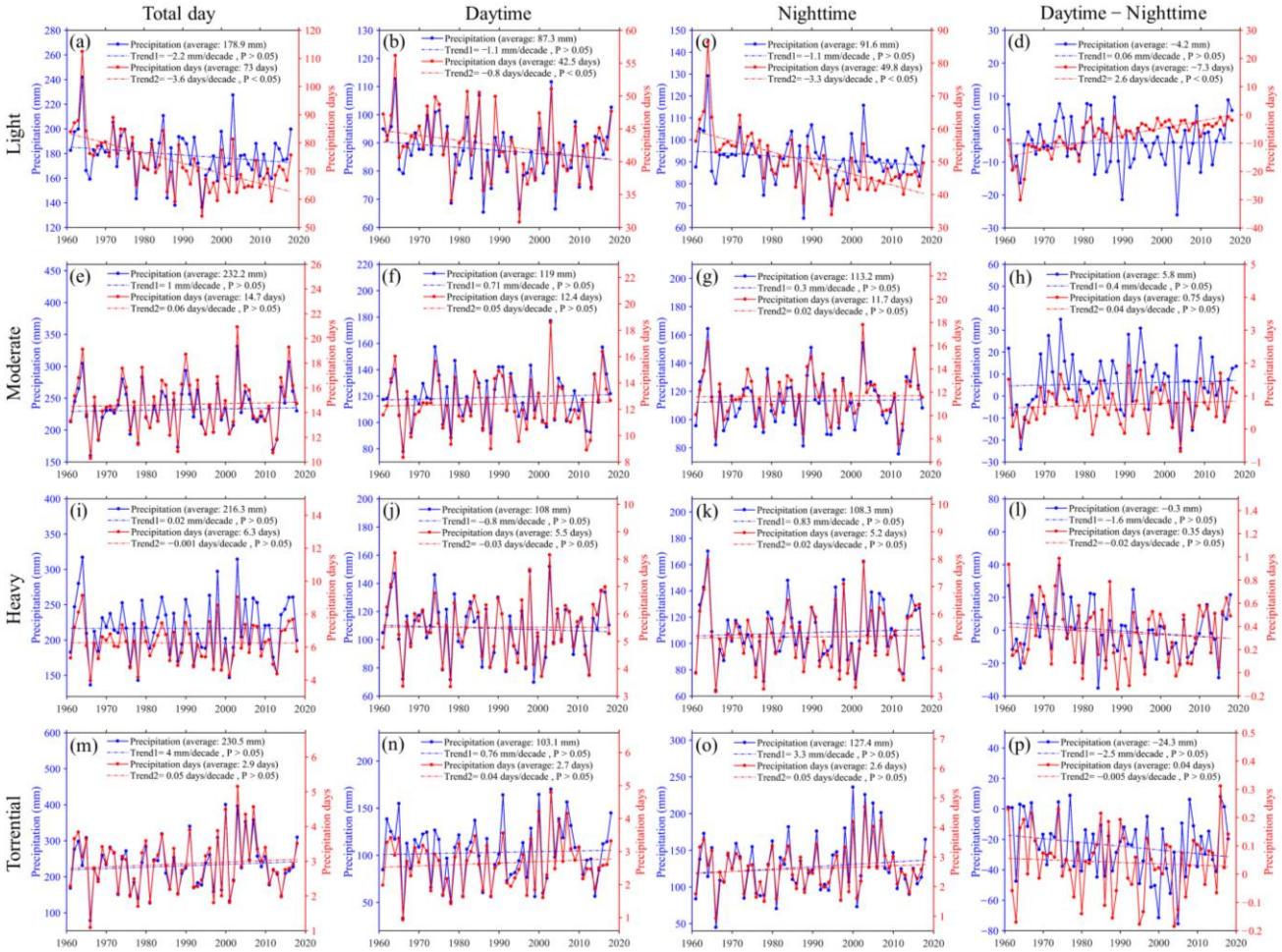

Figure 7. Time series (1961−2018) of the total, daytime, nighttime, and their difference (daytime minus nighttime) in terms of precipitation amount and days at different grades of intensity. The rows represent changes at different grades of precipitation intensity (light, moderate, heavy, and torrential), and the columns represent changes at different timescales (total, daytime, nighttime, and daytime minus nighttime).

The average of heavy precipitation was similar to that of moderate precipitation, but there were approximately half the number of heavy precipitation days compared with moderate precipitation days (Figure 7i). Total (days), daytime (days, Figure 7j), and nighttime precipitation (days, Figure 7k) at the heavy grade did not show obvious linear trend characteristics. Although the amount and days of daytime and nighttime precipitation at the heavy grade were basically similar, their differences showed slight downward trends, indicating that the contributions of nighttime precipitation to the total heavy precipitation was slightly greater (Figure 7l). As shown in Figure 7m, although the annual average torrential and moderate precipitation were basically similar, there were only 2.9 torrential precipitation days, which was 20% the number of moderate precipitation days. Both the amount and days of torrential precipitation showed slight upward trends, which were mainly caused by slight upward trends in daytime (Figure 7n) and nighttime (Figure 7o) precipitation events. As shown in Figure 7p, the average nighttime precipitation was 24.3 mm more than the daytime precipitation, but daytime and nighttime precipitation days were basically the same, which indicated that the precipitation intensity during the nighttime was greater than during the daytime at the torrential grade. The amount and days of the difference between daytime and nighttime precipitation at the torrential grade showed slight downward trends, indicating that the contributions of nighttime precipitation to the total torrential precipitation showed increasing trends.

The amount (Figure 8a) and days (Figure 8b) of light precipitation increased slightly in March to May compared with June. For the light grade, the daytime precipitation obviously exceeded the nighttime precipitation during July and August, but the number of daytime precipitation days did not significantly exceed the nighttime precipitation days. This indicated that the daytime precipitation intensity at the light grade during July and August was stronger than in the nighttime. As shown in Figure 8c, the seasonal cycles of the differences between daytime and nighttime precipitation (amount and days) at the light grade were relatively consistent. In August, the daytime precipitation amount and days at the light grade were higher than those in the nighttime. The seasonal cycles of moderate precipitation amount (Figure 8d) and days (Figure 8e) showed upward trends from January to July, and then showed downward trends after peaking in July. At the moderate grade in summer (June−August), the daytime precipitation amount and days exceeded those of the nighttime precipitation (Figure 8f). This indicated that moderate precipitation was more likely to occur in the daytime in the HRB during summer. The seasonal distributions of heavy precipitation were similar to those of moderate precipitation (Figure 8g–i), with the daytime precipitation amount and days increasing slightly compared with the nighttime precipitation during July and August. The kurtosis coefficients of the seasonal curves of torrential precipitation (Figure 8j,k) were obviously higher than those of mild, moderate, and heavy precipitation. This implied that torrential precipitation had more obvious seasonal characteristics (mainly occurring in summer). The differences between daytime and nighttime precipitation days at the torrential grade were very small, but the intensity of the daytime precipitation was less than that of the nighttime precipitation (negative values for the difference between daytime and nighttime precipitation amount), especially in summer (Figure 8l).

3.3. Proportions of Sub-Daily Precipitation under Extreme Precipitation Conditions

As shown in Figure 9, RX5day mainly occurred during June−September (90%), especially in July and August (64%). RX5day was most likely to occur in July (the largest proportion) in the HRB. The multiyear average value of RX5day was 151.5 mm, accounting for 17.8% of the annual total precipitation (Figure 10a). Neither RX5day nor its proportion of annual total precipitation presented a significant upward or downward trend. The daytime precipitation and the proportion under RX5day were 68.6 mm and 45.8%, respectively, with slight decreasing trends (Figure 10b). As shown in Figure 10c, the nighttime precipitation and the proportion under RX5day were 14.3 mm and 8.4% more than the daytime precipitation, respectively, with slight increasing trends.

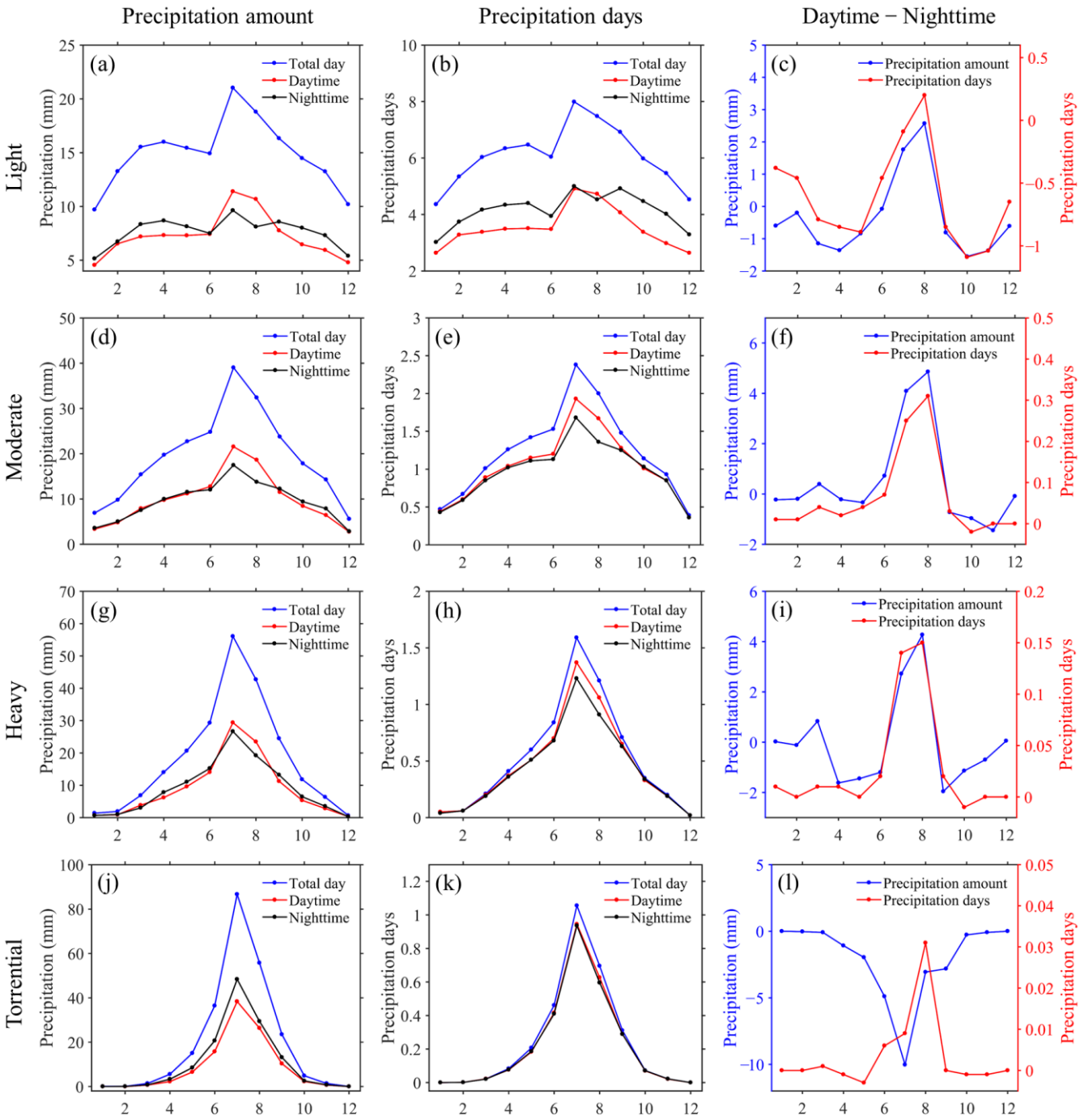

Figure 8. Seasonal cycles in the amount, days, and their difference (daytime minus nighttime) for total, daytime, and nighttime precipitation at different grades of intensity. The rows represent changes at different grades of precipitation intensity (light, moderate, heavy, and torrential), and the columns represent changes in different precipitation indices (precipitation amount, precipitation days, and daytime minus nighttime).

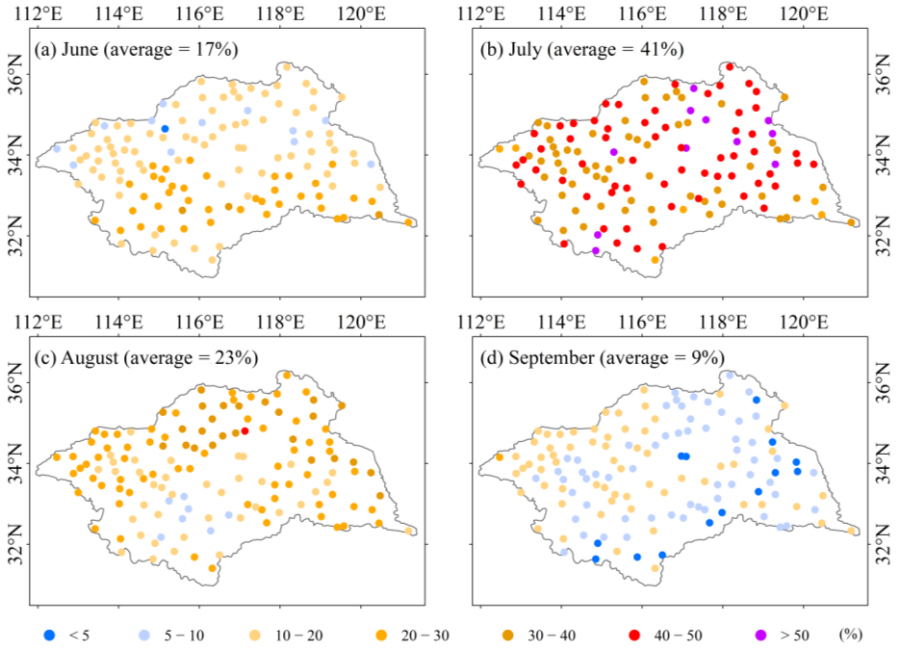

Figure 9. The spatial proportions of the (**a**) June, (**b**) July, (**c**) August, and (**d**) September in which RX5day occurs.

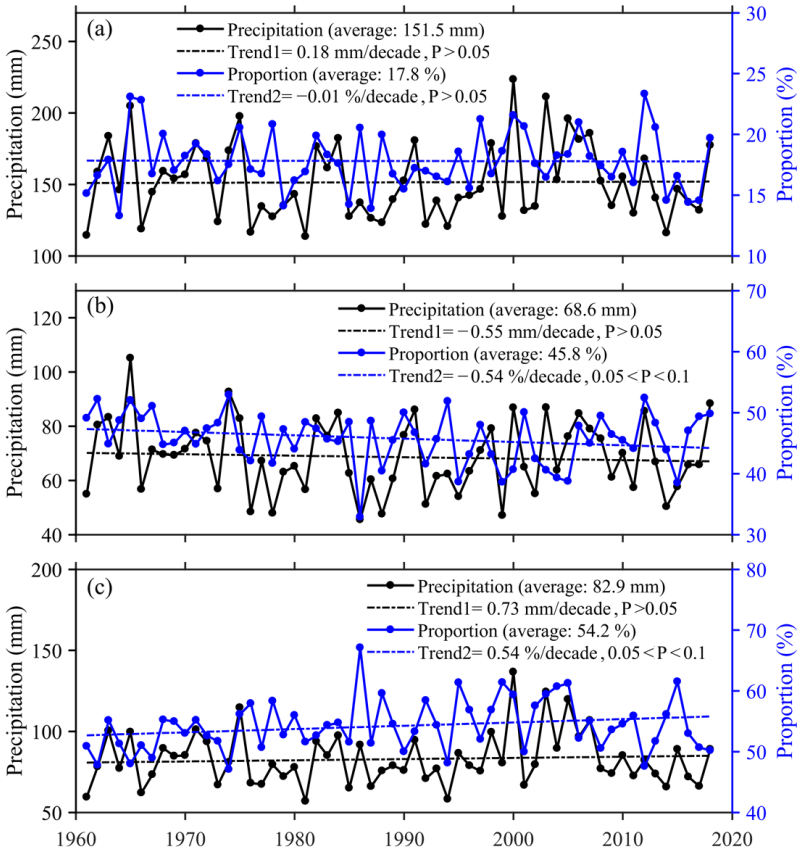

Figure 10. (**a**) Annual variations in RX5day precipitation and its proportion to the annual total precipitation. The amount and proportions of (**b**) daytime and (**c**) nighttime precipitation under RX5day conditions.

The multiyear averages of RX5day ranged from 130 to 175 mm (Figure 11a), and the values in the southwestern and southeastern parts (>160 mm) of the basin were greater

than those of other parts, indicating that the flood risks were higher in these two regions. RX5day showed the mixture of upward and downward trends in the HRB, and it failed generally to pass the $p < 0.05$ significance level. The ranges of daytime (Figure 11b) and nighttime (Figure 11c) precipitation under RX5day conditions were 55−85 mm and 75−90 mm, respectively, and both showed high values in the southwestern parts of the basin. Under RX5day conditions, the daytime precipitation presented a downward trend (four stations pass the $p < 0.05$ significance level), whereas the nighttime precipitation presented an upward trend (six stations pass the $p < 0.05$ significance level).

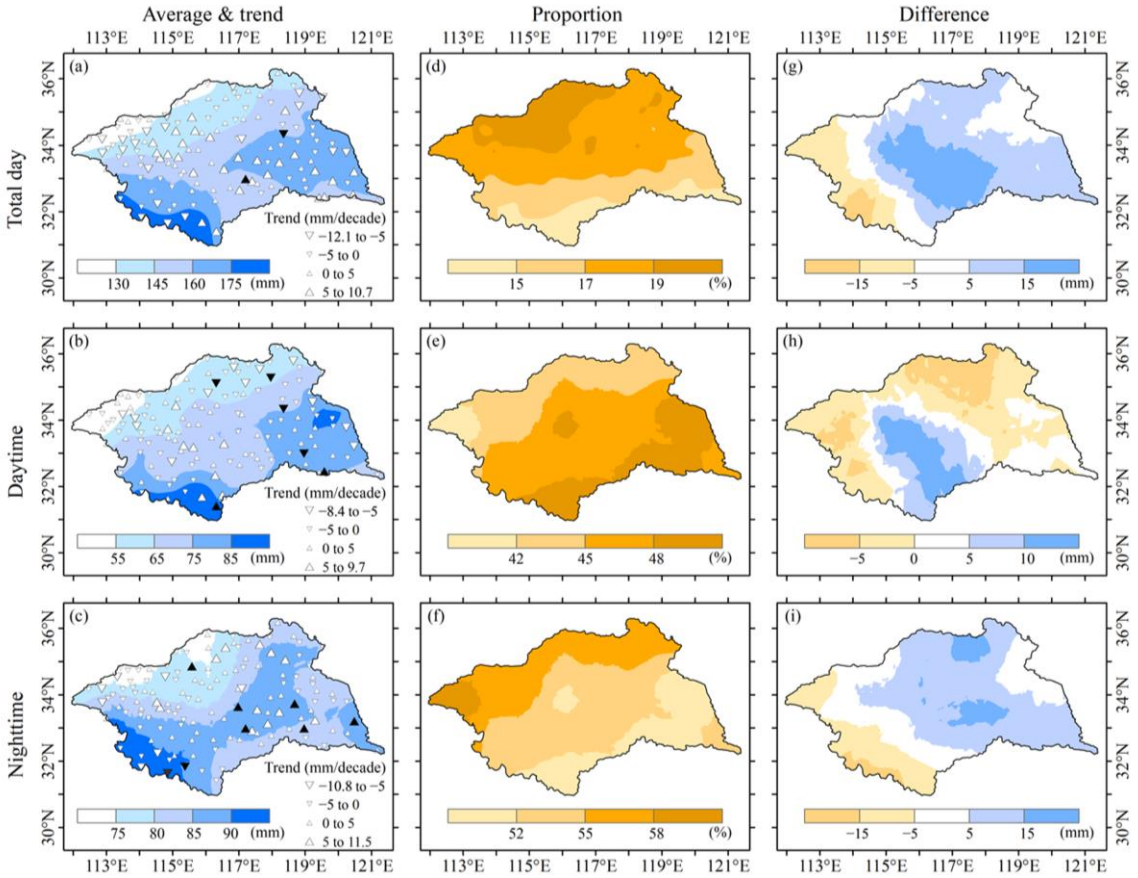

Figure 11. (**a**) Climatology of RX5day and trend characteristics, (**b**,**c**) the spatial patterns of daytime and nighttime precipitation under RX5day conditions. (**d**) The RX5day proportion of the annual total precipitation, and (**e**,**f**) the proportions of daytime and nighttime precipitation under RX5day conditions. (**g**) The mean differences between RX5day values in the two equal periods (1990–2018 minus 1961–1989), and (**h**,**i**) the mean differences between the two equal periods (1990–2018 minus 1961–1989) in the daytime and nighttime precipitation under RX5day conditions. Upward and downward triangles denote increase and decrease trends, respectively; solid triangles represent linear trends at the $p < 0.05$ significance level.

The RX5day proportion of the total annual precipitation decreased from >19% in the northern parts of the basin to <15% in the southern parts (Figure 11d). The proportion of daytime precipitation under RX5day conditions decreased from >48% in the southeast to <42% in the northwest (Figure 11e). The spatial proportion of nighttime precipitation under RX5day conditions was opposite to that of daytime (Figure 11f). In order to explore the variations in RX5day in terms of climatology, we divided the study period into two equal periods (1961–1989 and 1990–2018). The average of RX5day in the latter period (1990–2018) was overall greater than that in the earlier period (Figure 11g), especially in the central parts of the basin (>15 mm). For daytime precipitation under RX5day conditions, the positive values for the differences between 1990–2018 and 1961–1989 were mainly concentrated in

the central and southern parts of the basin (Figure 11h). As shown in Figure 11i, the areas with positive values for the differences in nighttime precipitation were larger than those for the daytime.

As shown in Figure 12, although the TR90p days only accounted for approximately 1/10 of the total precipitation days (all wet days), TR90p reached 1/2 of the total precipitation amount. Annual amount and days of TR90p showed slight upward trends. NR90p not only had larger annual averages (amount and days) than those of DR90p, but it also had greater increasing rates than those of DR90p, which indicated that more extreme precipitation was prone to occur during the nighttime.

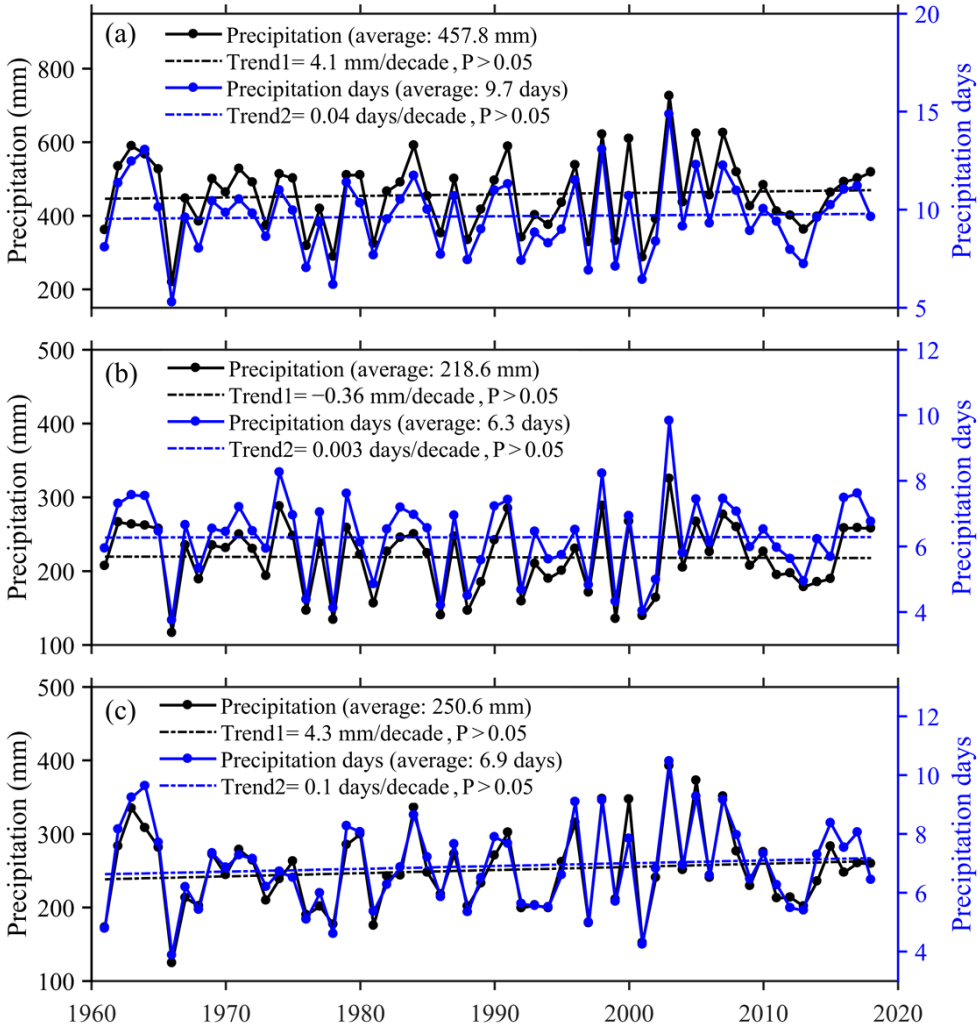

Figure 12. Annual variations in (**a**) TR90p, (**b**) DR90p, and (**c**) NR90p.

We analyzed the proportions of daytime and nighttime precipitation (amount and days) under TR90p conditions. As shown in Figure 13, TR90p produced 216.7 mm during the daytime and 241.2 mm during the nighttime, indicating that there was 5.4% more TR90p during the nighttime than during the daytime. Although the daytime and nighttime precipitation under TR90p conditions did not show significant upward or downward trends, their proportions showed significant downward trends during the daytime and significant upward trends during the nighttime from 1961 to 2018. We found that the proportions of daytime and nighttime precipitation under TR90p conditions underwent a turning point in 1999. The increasing rate in the proportion of daytime precipitation during 1999–2018 was approximately twice the decreasing rate during 1961–1999, whereas the decreasing rate in the proportion of nighttime precipitation during 1999–2018 was approximately twice the increasing rate during 1961–1999. These indicated that the proportion of TR90p during

the daytime was increasing, whereas the proportion during the nighttime was decreasing after 1999. In total, 88.2% of TR90p conditions occurred during the daytime and 84.2% occurred during the nighttime. The increasing rate in the proportion during the daytime was greater than the proportion during the nighttime from 1995 to 2018, which indicated that when TR90p occurs, the intensity of nighttime precipitation was stronger than that of daytime. This implied that the intensity of precipitation during the nighttime was greater than during the daytime when TR90p occurred.

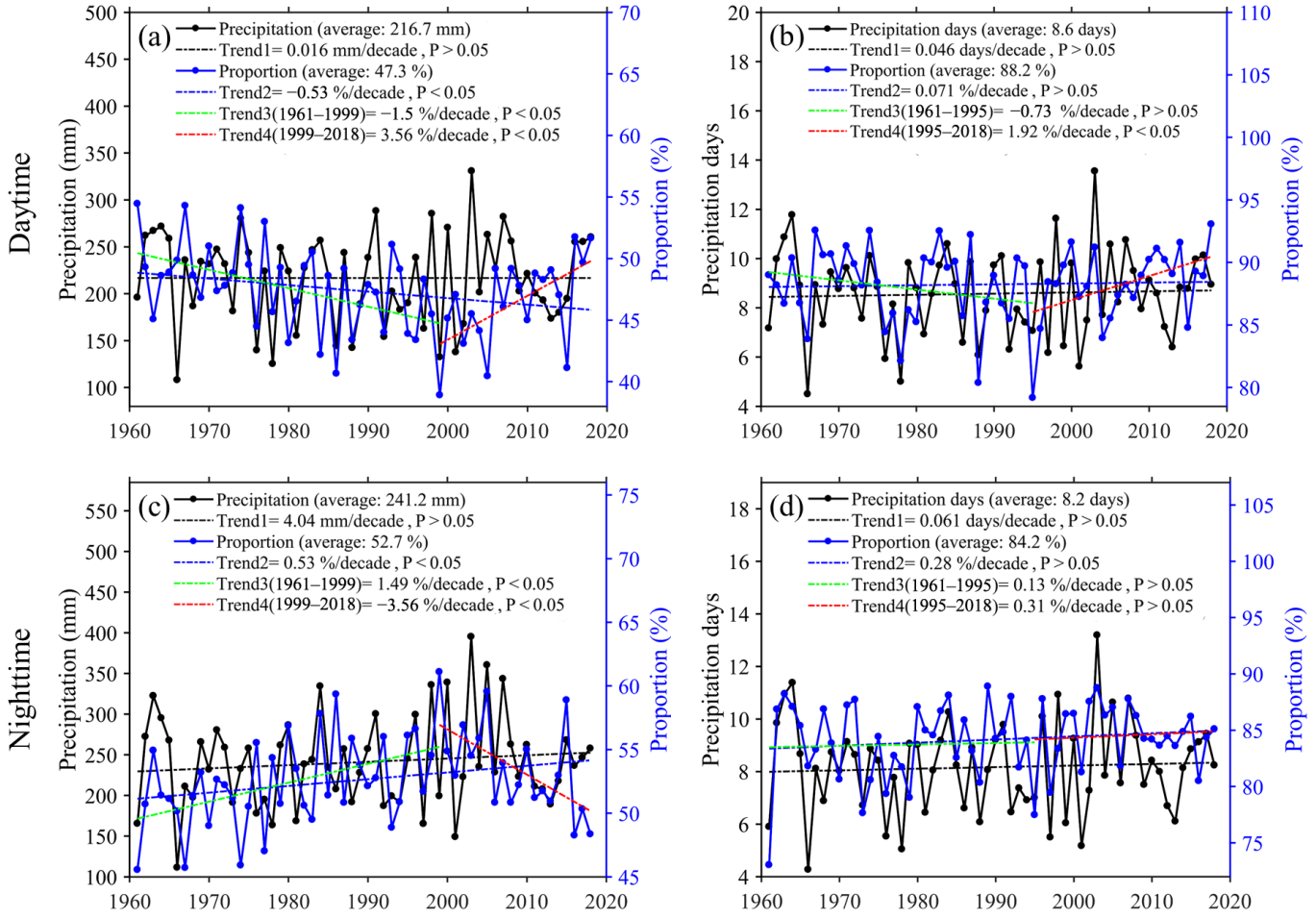

Figure 13. (**a**) Daytime precipitation under TR90p conditions and its proportion of TR90p. (**b**) Number of precipitation days under TR90p conditions and the proportion of TR90p. (**c**) Nighttime precipitation under TR90p conditions and its proportion of TR90p. (**d**) Number of precipitation nights under TR90p conditions and the proportion of TR90p.

The climatology of TR90p in the HRB ranged from >600 mm in the south to <400 mm in the north (Figure 14a). The TR90p in the latter period (1990–2018) was greater than that in the earlier period (1961–1989) in most areas of the basin (Figure 14b), especially in the central and southeastern parts of the basin (>50 mm). The spatial pattern of TR90p days was similar to that of the TR90p amount (Figure 14c), but their trends differed significantly. The spatial patterns of the difference of TR90p days between 1990–2018 and 1961–1989 were similar to those of the TR90p amount (Figure 14d), and the larger values were distributed in the central and southeastern parts of the basin (>0.6 days). The proportion of TR90p during the daytime was slightly higher in the south than in the northwest, and the stations reporting significant downward trends were concentrated in the northeast parts of the basin (Figure 14e). The average proportion of TR90p during the nighttime showed the opposite spatial pattern as during the daytime (Figure 14f), decreasing from >54% in the northern parts of the basin to <50% in the southern parts of the basin. The stations

reporting significant increasing trends in the proportion of TR90p during the nighttime were mainly concentrated in the northeastern parts of the basin. The proportions of daytime precipitation days under TR90p days were 83–91% (Figure 14g, high values in the southern parts of the basin), and the proportions of precipitation nights under TR90p days were 83–87% (Figure 14h, low values in the central parts of the basin). The proportion of daytime precipitation to TR90p showed significant downward trends in the eastern parts of the basin during 1961–1999 (Figure 14i), whereas the proportion of nighttime precipitation to TR90p showed significant upward trends (Figure 14j). The proportions of daytime precipitation days to TR90p days showed significant downward trends at only four stations during 1961–1995 (Figure 14k), whereas the proportions of precipitation nights to TR90p days showed significant upward trends at six stations (Figure 14l). The proportions of daytime precipitation to TR90p at 11 stations showed significant upward trends during 1999–2018 (Figure 14m), and the proportion of nighttime precipitation to TR90p at these 11 stations showed significant downward trends (Figure 14n). The proportions of daytime precipitation days to TR90p days at 10 stations showed significant upward trends during 1995–2018 (Figure 14o), whereas the proportions of precipitation nights to TR90p days showed significant increasing trends at only four stations (Figure 14p).

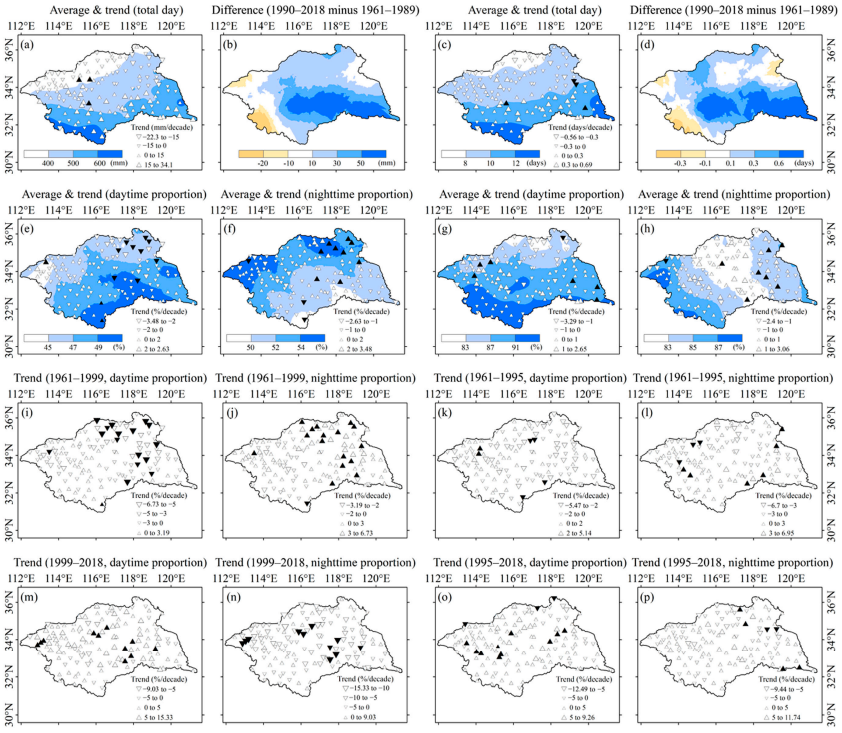

Figure 14. (**a**) Climatology and trend characteristics of TR90p during 1961–2018 and (**b**) the mean difference in TR90p between 1990–2018 and 1961–1989. (**c**) Climatology and trend characteristics of TR90p days during 1961–2018, (**d**) the mean difference in TR90p between 1990–2018 and 1961–1989. (**e**,**f**) Spatial proportions of the daytime and nighttime precipitation to TR90p, and (**g**,**h**) spatial proportions of the numbers of daytime and nighttime precipitation events to TR90p. (**i**,**j**) Spatial proportion trends of daytime and nighttime precipitation to TR90p during 1961–1999, and (**k**,**l**) spatial proportions of the numbers of daytime and nighttime precipitation events to TR90p during 1961–1995. (**m**,**n**) Spatial proportion trends of the daytime and nighttime precipitation to TR90p during 1999–2018, and (**o**,**p**) spatial proportions of the numbers of daytime and nighttime precipitation events to TR90p during 1995–2018. Upward and downward triangles denote increase and decrease trends, respectively; solid triangles represent linear trends at the $p < 0.05$ significance level.

The average of CEDNP was 94.3 mm, which accounted for 20% of TR90p (Figure 15a). Both CEDNP and its proportion to TR90p showed upward trends during 1961–2018. As

shown in Figure 15b, there was an average of 1.2 CEDNP days, accounting for 12% of the TR90p days. Both CEDNP days and its proportion to TR90p days showed increasing trends. Both daytime (Figure 15c) and nighttime (Figure 15d) precipitation and their proportions to CEDNP showed upward trends, and the trends during the nighttime were slightly greater than during the daytime.

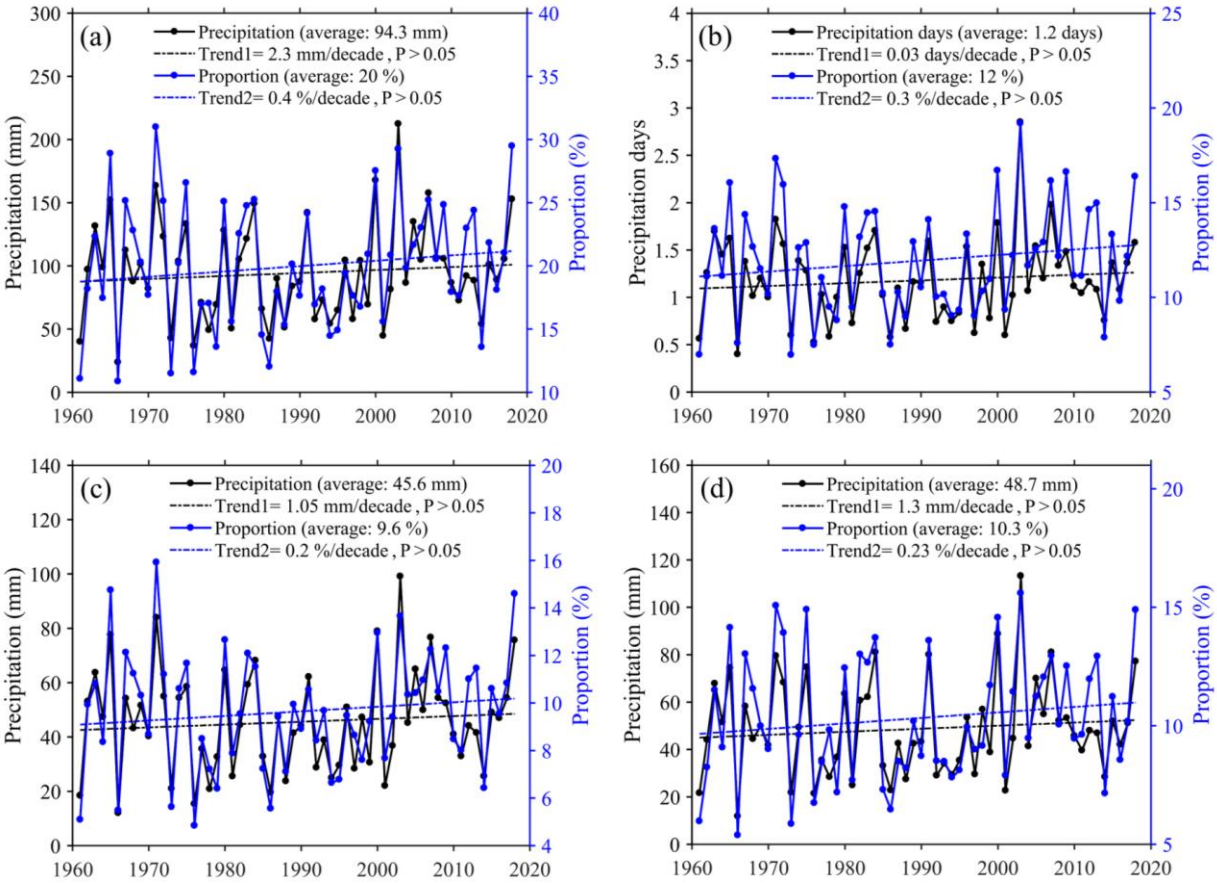

Figure 15. Annual variations in (**a**) CEDNP amount and its proportion to TR90p, (**b**) CEDNP days and its proportion to TR90p days, (**c**) daytime precipitation amount to CEDNP and its proportion to TR90p, and (**d**) nighttime precipitation to CEDNP and its proportion to TR90p.

The average CEDNP decreased from >150 mm in the southwestern parts of the basin to <50 mm in the northeastern parts of the basin (Figure 16a). There were significant increasing rates of >10 mm/decade at four stations. The proportion of CEDNP to TR90p decreased from >24% in the southwest to <12% in the northeast (Figure 16b), indicating that under extreme conditions of total daily precipitation, CEDNP was more likely to occur in the southwestern parts of the basin. The average value of CEDNP during 1990–2018 was overall greater than that during 1961–1989 (Figure 16c), especially in the southeastern parts of the basin (>20 mm). As shown in Figure 16d, the spatial pattern of the average CEDNP days was similar to that of CEDNP amount. CEDNP days showed significant increasing trends at eight stations, which had greater amount of CEDNP. The spatial proportion of CEDNP days to TR90p days was similar to that of CEDNP amount, decreasing from >15% in the southwest to <8% in the northeast (Figure 16e). The spatial pattern of the difference of CEDNP days between 1990–2018 and 1961–1989 was similar to that of CEDNP amount, but the positive value area was smaller than that of CEDNP amount (Figure 16f).

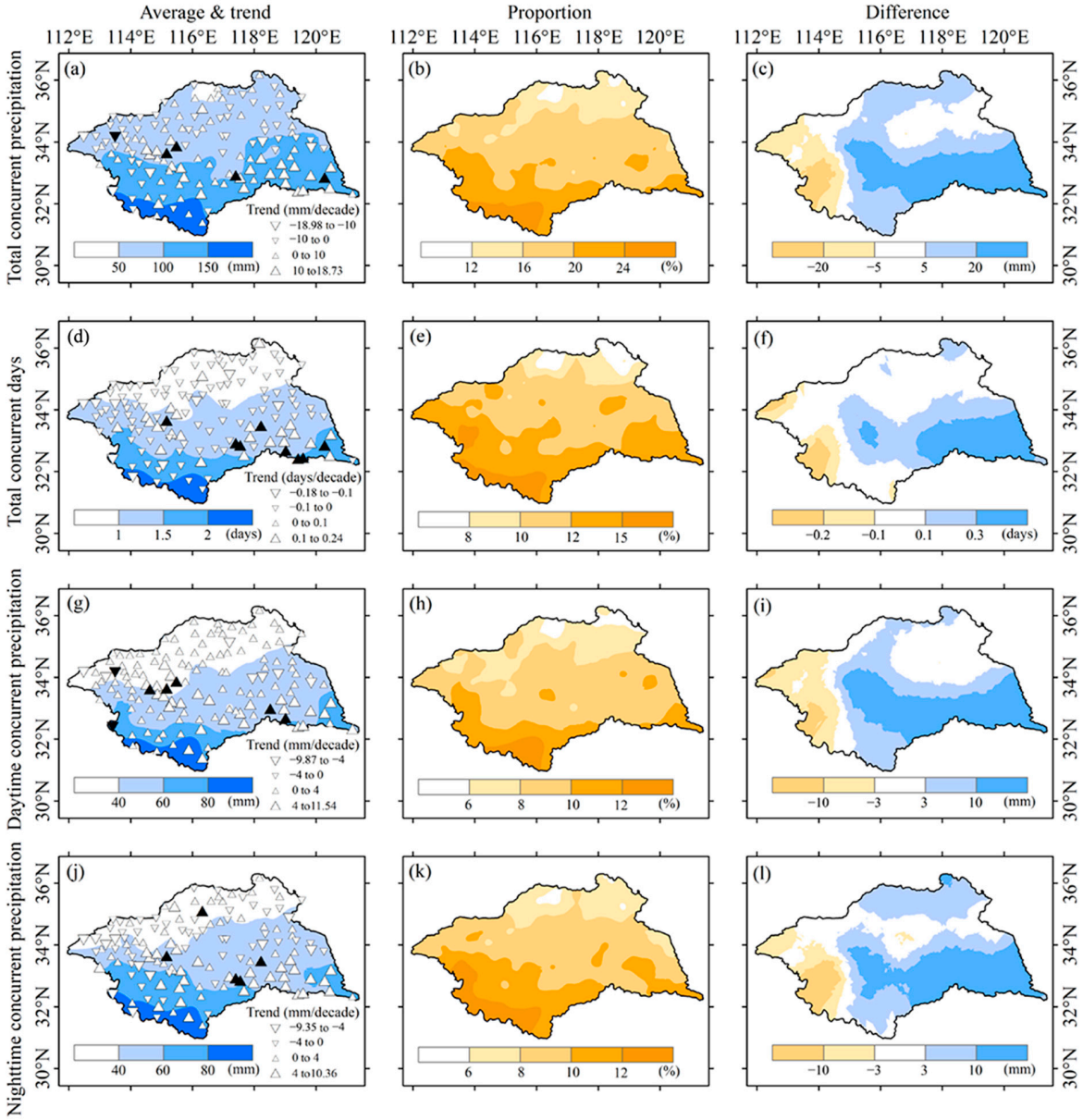

Figure 16. Spatial patterns of (**a**) mean CEDNP amount and trend (1961–2018), (**b**) the proportion of CEDNP amount to TR90p, and (**c**) the average difference of CEDNP amount between 1990–2018 and 1961–1989. (**d**–**f**) The same as (**a**–**c**), but for the CEDNP days. The spatial characteristics of (**g**) average daytime precipitation amount and trend under CEDNP, (**h**) the proportion of daytime precipitation amount to CEDNP under TR90p conditions, and (**i**) the average difference of daytime precipitation under CEDNP conditions between 1990–2018 and 1961–1989. (**j**–**l**) the same as (g–**i**), but for nighttime precipitation to CEDNP. Upward and downward triangles denote increase and decrease trends, respectively; solid triangles represent linear trends at the $p < 0.05$ significance level.

The average daytime precipitation under CEDNP condition showed a decrease from >80 mm in the southwest to <40 mm in the northeast, with five stations showing significant upward trends (Figure 16g). The proportion of daytime precipitation to CEDNP decreased from >12% in the southwest to <6% in the northeast (Figure 16h). The spatial pattern of the difference in daytime precipitation between 1990–2018 and 1961–1989 under CEDNP conditions revealed large values in the central and southeastern parts of the basin (Figure 16i). The spatial characteristics of the amount, trend, proportion, and difference (1990–2018 minus 1961–1989) of the nighttime precipitation to CEDNP were similar to those

of daytime precipitation, but the areas having large values were greater than that of the daytime precipitation (Figure 16j–l).

The average proportion of TR90p during spring was 16.6%, and it was >20% in the southern part of the basin (Figure 17a). The average proportion of TR90p during summer reached as high as 63.5%, with the northeastern part of the basin reaching >70% (Figure 17b). The average proportion of TR90p during autumn was 18.5% (Figure 17c), with high values (>20%) in the northwestern part of the basin. The proportion of TR90p during winter was only 1.4% (Figure 17d). The spatial–seasonal patterns of the proportions of DR90p were similar to those of TR90p (Figure 17e–h). The proportion difference between DR90p and TR90p during autumn was the greatest (2.3%) among the four seasons. The spatial–seasonal proportions of NR90p were similar to those of DR90p; the proportion in summer was 5.1% lower than that of DR90p, and the proportion in autumn was 3.6% higher than that of DR90p (Figure 17i–l). The spatial–seasonal proportions of CEDNP were similar to those of NR90p; the proportion in spring was 5.5% lower than that of NR90p, and the proportion in summer was 7.9% higher than that of NR90p (Figure 17m–p).

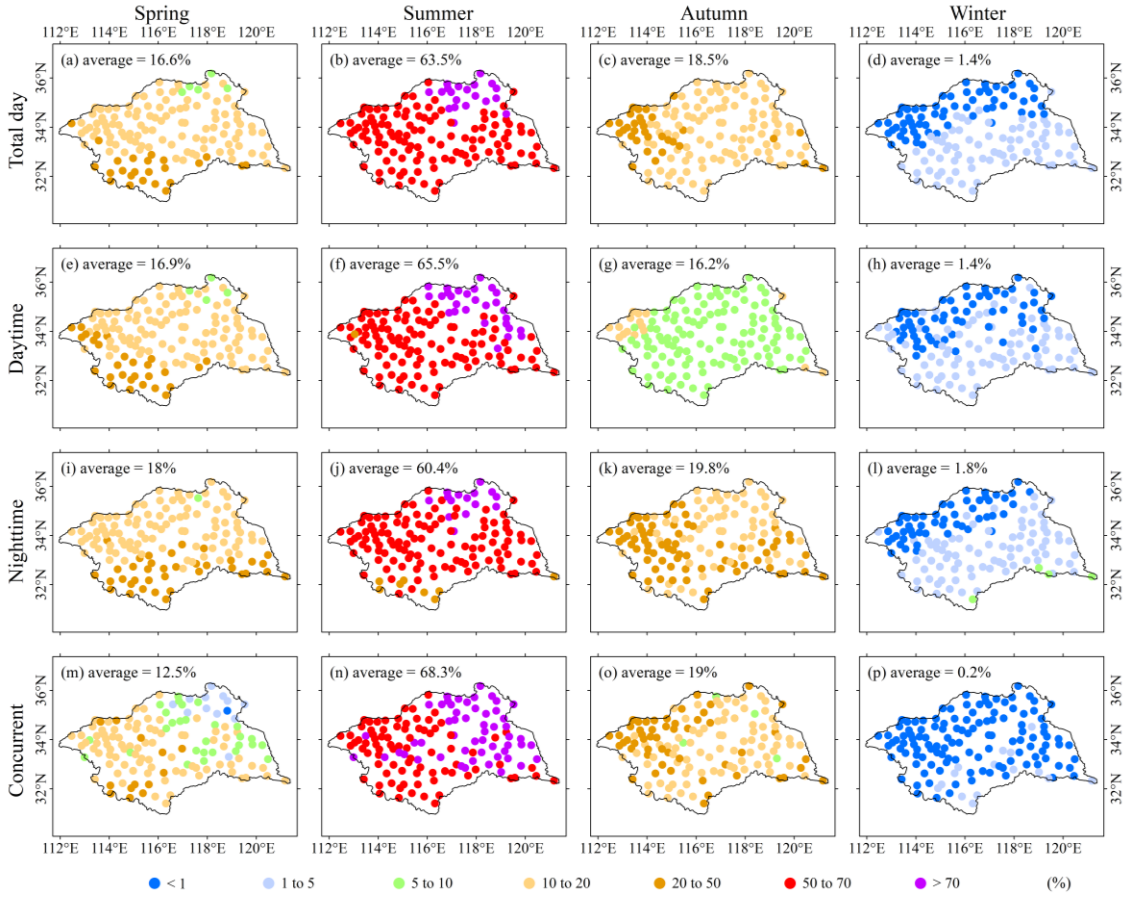

Figure 17. The proportions of (**a**–**d**) TR90p, (**e**–**h**) DR90p, (**i**–**l**) NR90p, and (**m**–**p**) CEDNP during spring (March–May), summer (June–August), autumn (September–November), and winter (December–February) compared with the whole year.

3.4. The Return Periods of CEDNP Events

Generalized Pareto fitting of daytime (Figure 18a) and nighttime (Figure 18b) precipitation under CEDNP conditions accounted for 98.5% and 96.3% of the total stations, respectively. The optimal marginal distribution function of the two variables (daytime and nighttime precipitation under CEDNP) were used to construct the joint distributions via the copula methods. As shown in Figure 18c, 11.9%, 21.5%, 22.2%, and 44.4% of the total stations conformed to Gaussian, Clayton, Frank, and Gumbel copulas.

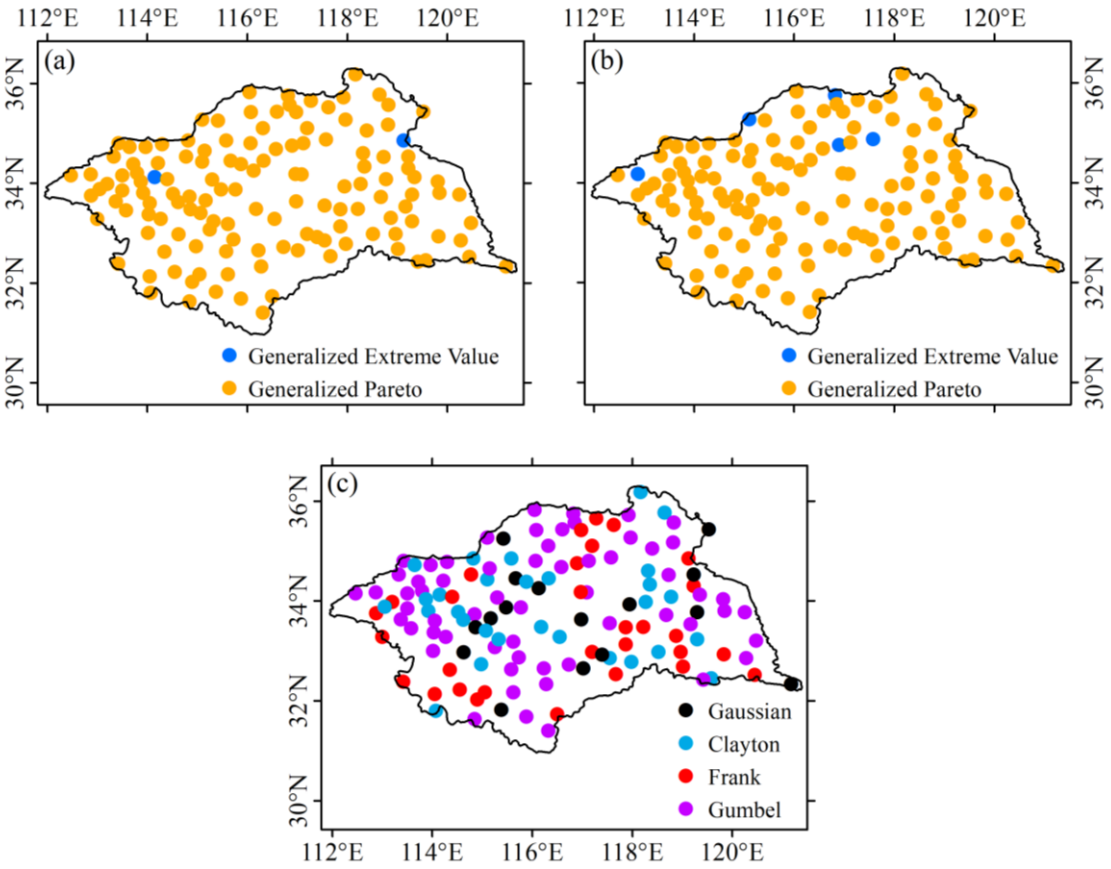

Figure 18. The selection of appropriate marginal distributions for (**a**) daytime and (**b**) nighttime precipitation under CEDNP conditions, and (**c**) their copulas.

We selected stations in different regions of the HRB to analyze the return periods of different combinations of daytime and nighttime precipitation under CEDNP conditions. These stations are located in the western (Xuchang in Henan Province), northern (Jining in Shandong Province), eastern (Lianshui in Jiangsu Province), and southern (Dingyuan in Anhui Province) areas of the HRB. As shown in Figure 19, the concurrent return periods for the daytime and nighttime precipitation of CEDNP events ranged from 5 to 100 years (contour lines). A CEDNP event in the upper right (lower left) corner in the contour lines of Figure 19 (each subplot) corresponded to the extreme (mild) conditions and had a longer (shorter) return period. Different combinations of daytime and nighttime precipitation under CEDNP conditions can produce the same return period at a given station. For example, at Xuchang station (Figure 19a), there were three CEDNP events in the 50-year return period isoline having different combinations of daytime and nighttime precipitation, namely X = 50.9 mm ∩ Y = 59.4 mm, X = 37.4 mm ∩ Y = 72.1 mm, and X = 26.7 mm ∩ Y = 83 mm have the same return period of 50 years (using X and Y as CEDNP daytime and nighttime precipitation, respectively). The same combination of daytime and nighttime precipitation has different return periods in different regions, which is shown in detail in Figure 20.

We divided the combinations of daytime and nighttime precipitation under CEDNP conditions into four grades to explore the characteristics of the return period with different CEDNP combinations. The four grades were G1 (X = 20 mm ∩ Y = 20 mm), G2 (X = 40 mm ∩ Y = 40 mm), G3 (X = 60 mm ∩ Y = 60 mm), and G4 (X = 80 mm ∩ Y = 80 mm). Under G1 conditions (Figure 20a), the range of the return periods was 1–2 years, and the return periods were shorter in the southern parts of the basin, indicating high risks of CEDNP events in this region. G2 (Figure 20b) was similar to G1 in spatial patterns, but the return period values increased (5–15 years). Under G3 conditions (Figure 20c), the risks of CEDNP events in the southwestern parts of the basin were relatively high (<20 years; a shorter

return period denotes a higher risk), whereas the return periods of the northwestern parts of the basin were relatively long (>80 years) under the same precipitation combination. As shown in Figure 20d, the return periods in most areas of the basin exceeded 100 years under G4 conditions.

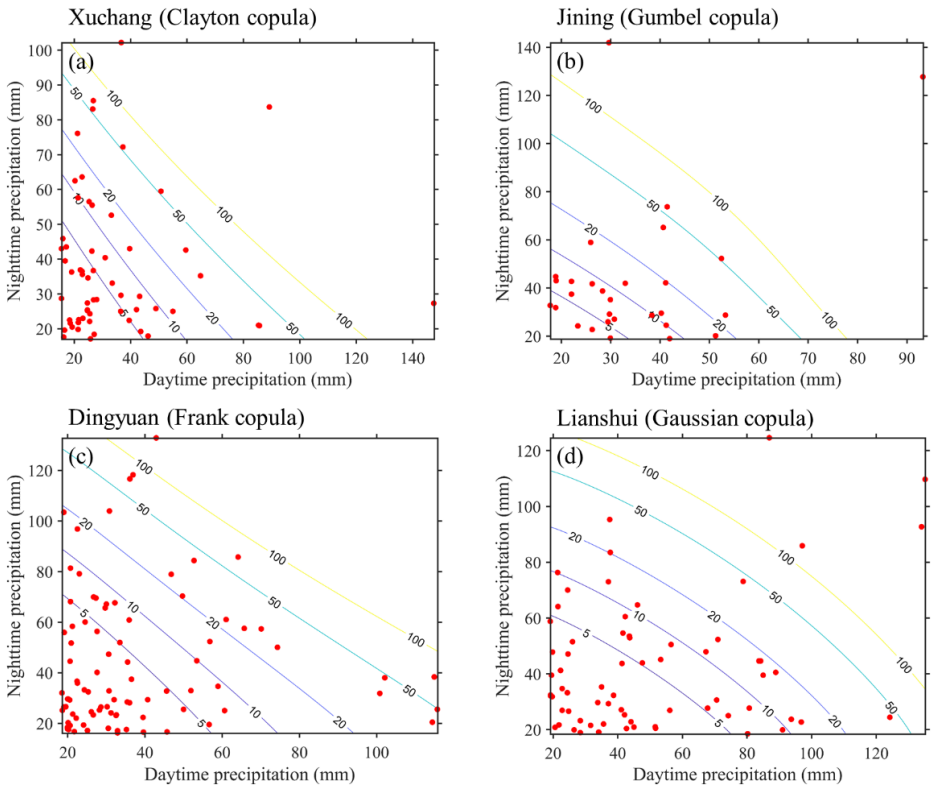

Figure 19. Joint return periods (years, contour lines) of daytime and nighttime precipitation under CEDNP conditions based on the copula method. The solid red dots denote CEDNP events. (**a**) Xuchang, (**b**) Jining, (**c**) Dingyuan, and (**d**) Lianshui are located in the western, northern, southern, and eastern parts of the HRB, respectively.

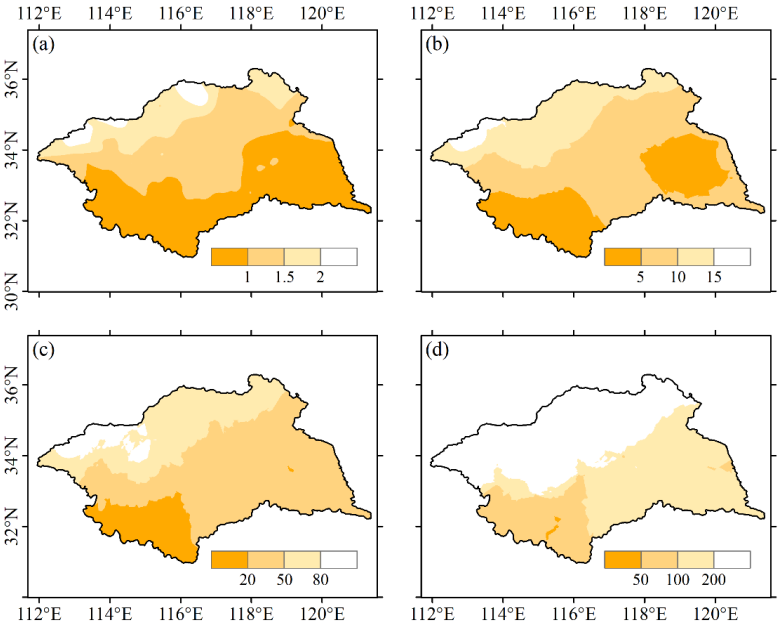

Figure 20. Spatial patterns of return periods (years) of (**a**) G1, (**b**) G2, (**c**) G3, and (**d**) G4 CEDNP events based on the copula method.

4. Discussion and Conclusions

Although there have been some studies of diurnal precipitation cycles on hourly scale [4,6,11,16,17], the proportions of daytime and nighttime precipitation (especially the proportions to extreme precipitation events) to the whole day play important roles in understanding the characteristics of the diurnal cycles of precipitation and water resources. This study explored the proportions of daytime and nighttime precipitation to daily total precipitation using data from 135 meteorological observation stations in the HRB.

ERA5 can reasonably capture the multi-year averages and variations of precipitation, but the long-term trend is insufficient, which was similar to the results of a previous study [53]. ERA5CON is better than ERA5 in capturing the precipitation characteristics, because ERA5 simulates more light precipitation days, especially during the daytime. This makes the average daytime precipitation in the HRB simulated by ERA5 more than that of nighttime precipitation, which is contrary to the observational data. The similar results have been proved by a previous study [3]. The nighttime precipitation in the HRB was slightly greater than the daytime precipitation. The peak of precipitation intensity in the afternoon (i.e., daytime) was stronger than that in the early morning (i.e., nighttime) in Shandong Province (the northern parts of HRB), but the precipitation amount in the afternoon was less than that in the early morning [6]. Generally, long-duration precipitation tends to occur around early morning, and short-duration precipitation tends to occur around afternoon [14,17,54], which results in a greater amount of precipitation during nighttime than during daytime. High precipitation amount in the HRB occur in the early morning and evening based on the hourly $0.1^\circ \times 0.1^\circ$ gridded precipitation dataset assimilated by 30,000 automatic meteorological stations in China during the summer of 2008−2016 [4]. Both the daytime and nighttime precipitation showed zonal distributions in the HRB, and the values in the southern parts of the basin were greater than those in the northern parts of the basin. This is because most of the HRB is flat and close to the sea; consequently, water vapor is generally imported by southerly summer monsoon winds and the total amount of water vapor continues to decrease during the process of transmission to the north [54]. Daytime and nighttime precipitation amount in the HRB were mainly concentrated in summer, which was similar to the findings of previous studies [4,6,16,54].

Wet seasons become wetter and dry seasons become drier on global averages, but this phenomenon may vary in different regions [21], especially for the range of precipitation difference between daytime and nighttime. The difference between daytime and nighttime precipitation in wet seasons showed a reversal of the upward trend after 2003 in the HRB. This was mainly due to the annual range of convective precipitation difference between daytime and nighttime during wet seasons. The linear trend in the differences between daytime and nighttime precipitation in dry seasons was not obvious, which was mainly attributable to the annual range of the large-scale precipitation difference between daytime and nighttime in the dry seasons.

The decreasing trends in light precipitation events (days) were mainly due to the significant decreasing trends in nighttime precipitation events in the HRB. The decreasing trends in light precipitation events with a low intensity are more obvious than light precipitation events with a high intensity [33]. Consequently, we can infer that the decreasing trends of nighttime precipitation events may be more obvious under conditions in which daily total light precipitation events have low. The slight upward trends of the moderate precipitation events were attributed to the slight upward trends of both daytime and nighttime precipitation events in the HRB, whereas the daytime precipitation during heavy precipitation events had a slight downward trend and the nighttime precipitation event had a slight upward trend. The contribution of nighttime precipitation events to torrential precipitation events was greater than that of daytime precipitation events in the HRB. As daily precipitation intensity increased, the seasonal cycles of total, day, and night precipitation were more obvious in the HRB. Some scholars have made similar conclusions in China [3,20]. Convective precipitation was prone to occur in the summer afternoon rather than in nighttime,

except for torrential precipitation in the HRB, resulting in greater precipitation in daytime during summer. Similar results have appeared in previous studies [10,54].

Both RX5day and TR90p are important indicators of extreme precipitation. RX5day accounts for approximately one-fifth of the annual total precipitation in the HRB. The TR90p days only accounted for approximately 10% of the annual total precipitation days, but the amount accounted for 50% of the annual total amount. RX5day and TR90p were more likely to occur in summer and were mainly affected by the Meiyu front and typhoons during this period [22,26]. Annual RX5day and TR90p amount showed slight upward trends, which were mainly caused by the increased nighttime precipitation. Similar results have been reported that the summer morning (afternoon) precipitation increased (decreased) in the area between the Yangtze and Yellow rivers [10]. Under RX5day conditions, the daytime precipitation showed downward trends, whereas the nighttime precipitation showed upward trends. Considering TR90p as the denominator, the proportion of daytime precipitation showed an upward turning trend during 1999−2018, whereas the proportion of nighttime precipitation showed a downward turning trend during this period. The proportion of RX5days to the total annual precipitation increased as the latitude increased in the HRB. Under both RX5day and TR90p conditions, large proportions of daytime precipitation were mainly concentrated in the southeastern parts of the HRB, whereas large proportions of nighttime precipitation were mainly concentrated in the northwestern parts of the basin. The values of RX5day and TR90p in 1990−2018 were larger in most parts of the HRB than in 1961−1989, indicating that extreme precipitation events increased in most parts of the basin.

In contrast with RX5day and TR90p, the increasing trends of CEDNP were caused by the increasing trends of both daytime and nighttime precipitation in the HRB. CEDNP showed that the value in the southwestern parts of the basin was greater than the value in the northeastern parts. The ratio of CEDNP (including daytime and nighttime precipitation under CEDNP conditions) to TR90p was large in the southwestern parts of the basin. This indicated that CEDNP events were prone to occur in the southwestern parts of the basin, which leads to high flood risks. The values of CEDNP in the central and southeastern parts of the HRB during 1990−2018 were higher than in 1961−1989. This was due to the increase in daytime and nighttime precipitation under CEDNP conditions, which led to increased risks of concurrent precipitation events in these regions.

The optimal distribution function for daytime and nighttime precipitation under CEDNP conditions in the HRB was basically the Generalized Pareto. Clayton, Frank, and Gumbel copulas accounted for approximately 90% of total stations in the HRB. These copula functions are also often used in the assessment of extreme precipitation risks [50,55,56]. For the same stations in the HRB, the return period of CEDNP event formed by the combination of different daytime and nighttime extreme precipitation may be the same. Similarly, for the same CEDNP, the return period of the CEDNP may differ owing to the different daytime and nighttime precipitation. If a univariate extreme precipitation is used to calculate the return period, then the risk of compound extreme precipitation may be underestimated. Based on the actual daytime and nighttime precipitation characteristics of the HRB, we used four combination (the case "∩") levels to evaluate the risks of concurrent extreme events under different combinations of daytime and nighttime precipitation. With the increase in daytime and nighttime precipitation, the risk of CEDNP in the southern part of the basin increased (shorter return period means higher risk), especially in the southwestern parts of the basin. The southern parts of the HRB generally have high economic and population density levels [57], and concurrent extremes markedly influence local economies and human health. The findings of this study provide a workable basis to make the government and local communities aware of the destructive impacts of concurrent precipitation extremes.

Author Contributions: Conceptualization, Y.Z. (Ying Zhu) and X.L.; methodology, Y.Z. (Yuqing Zhang); software, L.S.; validation, Y.Z. (Ying Zhu), Q.J. and C.C.; formal analysis, Y.Z. (Yuqing Zhang) and X.L.; investigation, Y.Z. (Ying Zhu) and L.S.; data curation, Y.Z. (Yuqing Zhang) and Q.J.; writing—review and editing, Y.Z. (Ying Zhu) and X.L.; supervision, T.Z. and P.X. All authors have read and agreed to the published version of the manuscript.

Funding: This study was jointly supported by the National Key R&D Program of China (2021YFC3201104), the National Natural Science Foundation of China (41907384, 52179013), the Humanities and Social Science Fund of Ministry of Education of China (19YJCZH259), the Huaishang Talent Foundation (42ZYQ00), the Belt and Road Special Foundation of the State Key Laboratory of Hydrology-Water Resources and Hydraulic Engineering (2021491011), the Natural Science Foundation of Anhui Province of China (1808085ME158, 2008085ME158), and the Key R&D Program of Anhui Province of China (No. 202004a06020016).

Institutional Review Board Statement: Not applicable.

Informed Consent Statement: Not applicable.

Data Availability Statement: The data that support our research findings are available from the corresponding author on request.

Acknowledgments: We are very grateful to the anonymous reviewers for their constructive comments and thoughtful suggestions.

Conflicts of Interest: The authors declare no conflict of interest.

References

1. Koutsoyiannis, D. Revisiting the global hydrological cycle: Is it intensifying? *Hydrol. Earth Syst. Sci.* **2020**, *24*, 3899–3932. [CrossRef]
2. Iliopoulou, T.; Koutsoyiannis, D. Projecting the future of rainfall extremes: Better classic than trendy. *J. Hydrol.* **2020**, *588*, 125005. [CrossRef]
3. Zhou, C.; Wang, K. Contrasting daytime and nighttime precipitation variability between observations and eight reanalysis products from 1979 to 2014 in China. *J. Clim.* **2017**, *30*, 6443–6464. [CrossRef]
4. Liu, J.; Yang, L.; Jiang, J.; Yuan, W.; Duan, Z. Mapping diurnal cycles of precipitation over China through clustering. *J. Hydrol.* **2021**, *592*, 125804. [CrossRef]
5. Dimitriadis, P.; Koutsoyiannis, D.; Iliopoulou, T.; Papanicolaou, P. A global-scale investigation of stochastic similarities in marginal distribution and dependence structure of key hydrological-cycle processes. *Hydrology* **2021**, *8*, 59. [CrossRef]
6. Zhuo, H.; Zhao, P.; Zhou, T. Diurnal cycle of summer rainfall in Shandong of eastern China. *Int. J. Climatol.* **2014**, *34*, 742–750. [CrossRef]
7. Cheng, Q.; Gao, L.; Zuo, X.; Zhong, F. Statistical analyses of spatial and temporal variabilities in total, daytime, and nighttime precipitation indices and of extreme dry/wet association with large-scale circulations of southwest China, 1961–2016. *Atmos. Res.* **2019**, *219*, 166–182. [CrossRef]
8. Sun, R.; Yuan, H.; Liu, X.; Jiang, X. Evaluation of the latest satellite–gauge precipitation products and their hydrologic applications over the huaihe river basin. *J. Hydrol.* **2016**, *536*, 302–319. [CrossRef]
9. Sun, R.; Yuan, H.; Liu, X. Effect of heteroscedasticity treatment in residual error models on model calibration and prediction uncertainty estimation. *J. Hydrol.* **2017**, *554*, 680–692. [CrossRef]
10. Yuan, W.; Yu, R.; Li, J. Changes in the diurnal cycles of precipitation over eastern China in the past 40 years. *Adv. Atmos. Sci.* **2013**, *30*, 461–467. [CrossRef]
11. Tsujimoto, K.; Ohta, T.; Aida, K.; Tamakawa, K.; Im, M.S. Diurnal pattern of rainfall in cambodia: Its regional characteristics and local circulation. *Prog. Earth Planet. Sci.* **2018**, *5*, 39. [CrossRef]
12. Ueno, K.; Takano, S.; Kusaka, H. Nighttime precipitation induced by a synoptic-scale convergence in the central tibetan plateau. *J. Meteorol. Soc. Jpn.* **2009**, *87*, 459–472. [CrossRef]
13. Chen, G.; Sha, W.; Iwasaki, T.; Ueno, K. Diurnal variation of rainfall in the yangtze river valley during the spring-summer transition from trmm measurements. *J. Geophys. Res. Atmos.* **2012**, *117*, D0610. [CrossRef]
14. Chen, H.; Yu, R.; Li, J.; Yuan, W.; Zhou, T. Why nocturnal long-duration rainfall presents an eastward-delayed diurnal phase of rainfall down the yangtze river valley. *J. Clim.* **2010**, *23*, 905–917. [CrossRef]
15. Cai, Y.; Lu, X.; Chen, G.; Yang, S. Diurnal cycles of mei-yu rainfall simulated over eastern China: Sensitivity to cumulus convective parameterization. *Atmos. Res.* **2018**, *213*, 236–251. [CrossRef]
16. Zhou, T.; Yu, R.; Chen, H.; Dai, A.; Pan, Y. Summer precipitation frequency, intensity, and diurnal cycle over China: A comparison of satellite data with rain gauge observations. *J. Clim.* **2008**, *21*, 3997–4010. [CrossRef]
17. Yu, R.; Xu, Y.; Zhou, T.; Li, J. Relation between rainfall duration and diurnal variation in the warm season precipitation over central eastern China. *Geophys. Res. Lett.* **2007**, *34*, L13703. [CrossRef]

18. Ye, H.; Fetzer, E.; Wong, S.; Lambrigtsen, B. Rapid decadal convective precipitation increase over eurasia during the last three decades of the 20th century. *Sci. Adv.* **2017**, *3*, e1600944. [CrossRef]
19. Miao, C.; Sun, Q.; Borthwick, A.G.L.; Duan, Q. Linkage between hourly precipitation events and atmospheric temperature changes over China during the warm season. *Sci. Rep.* **2016**, *6*, 22543. [CrossRef]
20. Li, Y.; Guo, B.; Wang, K.; Wu, G.; Shi, C. Performance of trmm product in quantifying frequency and intensity of precipitation during daytime and nighttime across China. *Remote Sens.* **2020**, *12*, 740. [CrossRef]
21. Chou, C.; Chiang, J.C.H.; Lan, C.W.; Chung, C.H.; Liao, Y.C.; Lee, C.J. Increase in the range between wet and dry season precipitation. *Nat. Geosci.* **2013**, *6*, 263–267. [CrossRef]
22. Jiong, C.; Yongguang, Z.; Xiaoling, Z.; Peijun, Z.H.U. Distribution and diurnal variation of warm-season short-duration heavy rainfall in relation to the mcss in China. *J. Meteorol. Res.* **2013**, *27*, 868–888. [CrossRef]
23. Zhang, S.; Ma, Z.; Li, Z.; Zhang, P.; Liu, Q.; Nan, Y.; Zhang, J.; Hu, S.; Feng, Y.; Zhao, H. Using cygnss data to map flood inundation during the 2021 extreme precipitation in henan province, China. *Remote Sens.* **2021**, *13*, 5181. [CrossRef]
24. Zhang, Y.; Sun, X.; Chen, C. Characteristics of concurrent precipitation and wind speed extremes in China. *Weather Clim. Extrem.* **2021**, *32*, 100322. [CrossRef]
25. Luo, L.; Xiao, H.; Yang, H.; Chen, H.; Guo, J.; Sun, Y.; Feng, L. Raindrop size distribution and microphysical characteristics of a great rainstorm in 2016 in Beijing, China. *Atmos. Res.* **2020**, *239*, 104895. [CrossRef]
26. Zhao, Y.; Huang, A.; Kan, M.; Dong, X.; Yu, X.; Wu, Y.; Zhang, X.; Cai, S. Characteristics of hourly extreme precipitation along the yangtze river basin, China during warm season. *Sci. Rep.* **2020**, *10*, 5613. [CrossRef] [PubMed]
27. Qiao, S.; Chen, D.; Wang, B.; Cheung, H.-N.; Liu, F.; Cheng, J.; Tang, S.; Zhang, Z.; Feng, G.; Dong, W. The longest 2020 meiyu season over the past 60 years: Subseasonal perspective and its predictions. *Geophys. Res. Lett.* **2021**, *48*, e2021GL093596. [CrossRef]
28. Xia, R.; Luo, Y.; Zhang, D.-L.; Li, M.; Bao, X.; Sun, J. On the diurnal cycle of heavy rainfall over the sichuan basin during 10–18 august 2020. *Adv. Atmos. Sci.* **2021**, *38*, 2183–2200. [CrossRef]
29. Huang, H.; Cui, H.; Ge, Q. Assessment of potential risks induced by increasing extreme precipitation under climate change. *Nat. Hazards* **2021**, *108*, 2059–2079. [CrossRef]
30. Fagnant, C.; Gori, A.; Sebastian, A.; Bedient, P.B.; Ensor, K.B. Characterizing spatiotemporal trends in extreme precipitation in southeast texas. *Nat. Hazards* **2020**, *104*, 1597–1621. [CrossRef]
31. Xie, W.; Zhou, B.; You, Q.; Zhang, Y.; Ullah, S. Observed changes in heat waves with different severities in China during 1961–2015. *Theor. Appl. Climatol.* **2020**, *141*, 1529–1540. [CrossRef]
32. Aghakouchak, A.; Cheng, L.; Mazdiyasni, O.; Farahmand, A. Global warming and changes in risk of concurrent climate extremes: Insights from the 2014 california drought. *Geophys. Res. Lett.* **2015**, *41*, 8847–8852. [CrossRef]
33. Zhang, Y.; Liu, C.; You, Q.; Chen, C.; Xie, W.; Ye, Z.; Li, X.; He, Q. Decrease in light precipitation events in huai river eco-economic corridor, a climate transitional zone in eastern China. *Atmos. Res.* **2019**, *226*, 240–254. [CrossRef]
34. Gao, C.; Li, X.; Sun, Y.; Zhou, T.; Luo, G.; Chen, C. Water requirement of summer maize at different growth stages and the spatiotemporal characteristics of agricultural drought in the huaihe river basin, China. *Theor. Appl. Climatol.* **2019**, *136*, 1289–1302. [CrossRef]
35. Zhang, W.; Pan, S.; Cao, L.; Cai, X.; Zhang, K.; Xu, Y.; Xu, W. Changes in extreme climate events in eastern China during 1960–2013: A case study of the huaihe river basin. *Quat. Int.* **2015**, *380–381*, 22–34. [CrossRef]
36. Sun, P.; Zhang, Q.; Yao, R.; Wen, Q. Hydrological drought regimes of the huai river basin, China: Probabilistic behavior, causes and implications. *Water* **2019**, *11*, 2390. [CrossRef]
37. Hersbach, H.; Bell, B.; Berrisford, P.; Hirahara, S.; Horányi, A.; Muñoz-Sabater, J.; Nicolas, J.; Peubey, C.; Radu, R.; Schepers, D.; et al. The era5 global reanalysis. *Q. J. R. Meteorol. Soc.* **2020**, *146*, 1999–2049. [CrossRef]
38. Owen, L.E.; Catto, J.L.; Stephenson, D.B.; Dunstone, N.J. Compound precipitation and wind extremes over europe and their relationship to extratropical cyclones. *Weather. Clim. Extrem.* **2021**, *33*, 100342. [CrossRef]
39. Zhang, Y.; Mao, G.; Chen, C.; Shen, L.; Xiao, B. Population exposure to compound droughts and heatwaves in the observations and era5 reanalysis data in the gan river basin, China. *Land* **2021**, *10*, 1021. [CrossRef]
40. Chinita, M.J.; Richardson, M.; Teixeira, J.; Miranda, P.M.A. Global mean frequency increases of daily and sub-daily heavy precipitation in era5. *Environ. Res. Lett.* **2021**, *16*, 074035. [CrossRef]
41. Liu, B.; Xu, M.; Henderson, M. Where have all the showers gone? Regional declines in light precipitation events in China, 1960–2000. *Int. J. Climatol.* **2011**, *31*, 1177–1191. [CrossRef]
42. Zhai, P.; Sun, A.; Ren, F.; Liu, X.; Gao, B.; Zhang, Q. Changes of climate extremes in China. *Clim. Chang.* **1999**, *42*, 203–218. [CrossRef]
43. Zhang, Y.; Yang, X.; Chen, C. Substantial decrease in concurrent meteorological droughts and consecutive cold events in huai river basin, China. *Int. J. Climatol.* **2021**, *41*, 6065–6083. [CrossRef]
44. Sklar, A. Random variables, joint distribution functions, and copulas. *Kybernetika* **1973**, *9*, 449–460.
45. Sadegh, M.; Ragno, E.; AghaKouchak, A. Multivariate copula analysis toolbox (mvcat): Describing dependence and underlying uncertainty using a bayesian framework. *Water Resour. Res.* **2017**, *53*, 5166–5183. [CrossRef]
46. Sadegh, M.; Moftakhari, H.; Gupta, H.V.; Ragno, E.; Mazdiyasni, O.; Sanders, B.; Matthew, R.; AghaKouchak, A. Multihazard scenarios for analysis of compound extreme events. *Geophys. Res. Lett.* **2018**, *45*, 5470–5480. [CrossRef]

47. Zhang, Y.; You, Q.; Mao, G.; Chen, C.; Li, X.; Yu, J. Flash drought characteristics by different severities in humid subtropical basins: A case study in the gan river basin, China. *J. Clim.* **2021**, *34*, 7337–7357. [CrossRef]
48. Schwarz, G. Estimating the dimension of a model. *Ann. Stat.* **1978**, *6*, 461–464. [CrossRef]
49. Li, X.; Ren, G.; Wang, S.; You, Q.; Sun, Y.; Ma, Y.; Wang, D.; Zhang, W. Change in the heatwave statistical characteristics over China during the climate warming slowdown. *Atmos. Res.* **2021**, *247*, 105152. [CrossRef]
50. Miao, C.; Sun, Q.; Duan, Q.; Wang, Y. Joint analysis of changes in temperature and precipitation on the loess plateau during the period 1961–2011. *Clim. Dyn.* **2016**, *47*, 3221–3234. [CrossRef]
51. Chang, J.; Li, Y.; Wang, Y.; Yuan, M. Copula-based drought risk assessment combined with an integrated index in the wei river basin, China. *J. Hydrol.* **2016**, *540*, 824–834. [CrossRef]
52. Zeng, Z.; Ziegler, A.D.; Searchinger, T.D.; Yang, L.; Chen, A.; Ju, K.; Piao, S.; Li, L.; Ciais, P.; Chen, D. A reversal in global terrestrial stilling and its implications for wind energy production. *Nat. Clim. Chang.* **2019**, *9*, 979–985. [CrossRef]
53. Jiao, D.; Xu, N.; Yang, F.; Xu, K. Evaluation of spatial-temporal variation performance of era5 precipitation data in China. *Sci. Rep.* **2021**, *11*, 17956. [CrossRef] [PubMed]
54. Mu, X.; Huang, A.; Wu, Y.; Xu, Q.; Zheng, Y.; Lin, H.; Fang, D.; Zhang, X.; Tang, Y.; Cai, S. Characteristics of the precipitation diurnal variation and underlying mechanisms over jiangsu, eastern China, during warm season. *Front. Earth Sci.* **2021**, *9*, 703071. [CrossRef]
55. Li, H.; Wang, D.; Singh, V.P.; Wang, Y.; Wu, J.; Wu, J.; Liu, J.; Zou, Y.; He, R.; Zhang, J. Non-stationary frequency analysis of annual extreme rainfall volume and intensity using archimedean copulas: A case study in eastern China. *J. Hydrol.* **2019**, *571*, 114–131. [CrossRef]
56. Bargaoui, Z.K.; Bardossy, A. Modeling short duration extreme precipitation patterns using copula and generalized maximum pseudo-likelihood estimation with censoring. *Adv. Water Resour.* **2015**, *84*, 1–13. [CrossRef]
57. Zhang, M.; Zhang, K.; Hu, W.; Zhu, B.; Wang, P.; Wei, Y. Exploring the climatic impacts on residential electricity consumption in Jiangsu, China. *Energy Policy* **2020**, *140*, 111398. [CrossRef]